HHS Public Access

Author manuscript

Nucl Med Biol. Author manuscript; available in PMC 2022 March 01.

Published in final edited form as:

Nucl Med Biol. 2021 ; 94-95: 67–80. doi:10.1016/j.nucmedbio.2021.01.002.

Synthesis and Preliminary Evaluation of ^{211}At-labeled Inhibitors of Prostate-Specific Membrane Antigen for Targeted Alpha Particle Therapy of Prostate Cancer

Ganesan Vaidyanathan[a], **Ronnie C. Mease**[b], **Il Minn**[b], **Jaeyeon Choi**[a], **Ying Chen**[b], **Hassan Shallal**[b], **Choong Mo Kang**[a], **Darryl McDougald**[a], **Vivek Kumar**[b], **Martin G. Pomper**[b], **Michael R. Zalutsky**[a,*]

[a]Department of Radiology, Duke University Medical Center, Durham, North Carolina [b]Russell H. Morgan Department of Radiology and Radiological Science, Johns Hopkins University School of Medicine, Baltimore, Maryland

Abstract

Introduction: The high potency and short tissue range of α-particles are attractive features for targeted radionuclide therapy, particularly for cancers with micro-metastases. In the current study, we describe the synthesis of a series of ^{211}At-labeled prostate-specific membrane antigen (PSMA) inhibitors and their preliminary evaluation as potential agents for metastatic prostate cancer treatment.

Methods: Four novel Glu-urea based PSMA ligands containing a trimethyl stannyl group were synthesized and labeled with ^{211}At, and for comparative purposes, ^{131}I, via halodestannylation reactions with *N*-chlorosuccinimide as the oxidant. A PSMA inhibitory assay was performed to evaluate PSMA binding of the unlabeled, iodinated compounds. A series of paired-label biodistribution experiments were performed to compare each ^{211}At-labeled PSMA ligand to its ^{131}I-labeled counterpart in mice bearing subcutaneous PC3 PSMA+ PIP xenografts.

Results: Radiochemical yields ranged from 32% to 65% for the ^{211}At-labeled PSMA inhibitors and were consistently lower than those obtained with the corresponding ^{131}I-labeled analogue. Good localization in PC3 PSMA+ PIP but not control xenografts was observed for all labeled molecules studied, which exhibited a variable degree of in vivo dehalogenation as reflected by thyroid and stomach activity levels. Normal tissue uptake and in vivo stability for several of the compounds was markedly improved compared with the previously evaluated compounds, [^{211}At]DCABzL and [*I]DCIBzL.

*Corresponding Author: Michael R. Zalutsky, Duke University, Bryan Research Building, 311 Research Drive, Durham, North Carolina 27710, USA. Tel: +1 919 684-7708; Fax: +1 919 684-7122; zalut001@mc.duke.edu.

Declaration of competing interest

G.V., R.M., I.L., M.P. and M.R.Z. are co-inventors on filed patent applications that cover ^{211}At- and ^{131}I-labeled PSMA inhibitors including the molecules comprising this study. We declare no other competing interests related to this work.

Conclusions and Implications for Patient Care: Compared with the first generation compound [^{211}At]DCABzL, several of the novel ^{211}At-labeled PSMA ligands exhibited markedly improved stability in vivo and higher tumor-to-normal tissue ratios. [^{211}At]GV-620 has the most promising characteristics and warrants further evaluation as a targeted radiotherapeutic for prostate cancer.

Graphical abstract

Keywords

Astatine; alpha emitter; prostate-specific membrane antigen; prostate cancer; radionuclide therapy

1. Introduction

Despite the development of new options for the treatment of metastatic castrate-resistant prostate cancer (mCRPC), the treatment of patients with mCRPC remains challenging [1]. One strategy that shows particular promise is targeted radionuclide therapy (TRT), building on the effectiveness of external beam therapy, a standard therapy for prostate-confined disease due in part to its radiosensitivity. Substituting anatomical targeting with biological targeting offers the possibility of extending its effectiveness from localized prostate cancer to the treatment of mCRPC. Initial studies were mainly focused on treatment of patients with bone metastases with β-particle emitting calcium and phosphonate analogues including ^{89}Sr chloride [2] and ^{153}Sm-SDTMP [3]. Although these agents provided proof of concept for TRT in mCRPC, they suffer from two significant limitations – they are at best palliative and not curative, and their uptake mechanism is not suited to treatment of soft tissue lesions.

A promising strategy for addressing these limitations is to exploit the high level and nearly universal expression of prostate-specific membrane antigen (PSMA) on prostate cancers, particularly those with the most malignant phenotype [4]. Although antibodies and antibody fragments have been used as the targeting vector, the most promising results have been obtained with low molecular weight (generally, < 1 kDa) PSMA-specific ligands labeled with a variety of radionuclides [5]. This work is exemplified by its most clinically mature example – a Phase III multi-center trial with β-particle emitting ^{177}Lu-labeled PSMA-617 (VISION trial – NCT03511664). That trial has not reached final readout at this time; in a Phase II trial with this radiotherapeutic in patients selected in part by PSMA PET imaging, about 40% exhibited reductions in tumor volume 3 months after treatment [6]. However, there have been reports of dose limiting hematologic toxicity with some ^{177}Lu-labeled PSMA inhibitors resulting in about 30% of patients being non-responders [7]. As noted in a recent review [5], because of their relatively long range in tissue, a β-particle decay that occurs in a bone metastasis can deposit a significant fraction of its decay energy in neighboring red marrow, potentially leading to a toxic effect.

An attractive approach to circumventing that problem is to utilize radiation with a more constrained range such as an α-emitter. The merit of this approach has been demonstrated in the context of bone seeking agents – use of ^{223}Ra instead of β-emitting alternatives resulted in a considerable reduction in hematological toxicity [8]. The shorter α-particle range also should have clear advantages for the treatment of micro-metastases that are frequently present in mCRPC. Moreover, α-particles have considerably higher potency than β-particles due to the generation of largely irreparable double-strand DNA breaks. Also, the efficacy of α-particles is dependent on neither the presence of oxygen nor on cell-cycle position [9].

A clinical study with ^{225}Ac-labeled PSMA-617 reported significant responses even in patients that did not respond to its ^{177}Lu-labeled analogue, demonstrating the promise of targeted α-particle therapy (TAT) in combination with a low-molecular-weight PSMA inhibitor [10]. However, quality of life after that treatment was frequently compromised by permanent xerostomia and lacrimal gland damage, with many of these patients dropping out of the study before receiving all of their scheduled doses of ^{225}Ac-labeled PSMA-617. The fact that ^{225}Ac emits four α-particles per decay likely contributes to its excellent therapeutic

effectiveness but also to its normal toxicity because the in vivo fate of its radioactive daughters is difficult to control.

We have been pursuing ^{211}At, which emits only one α-particle per decay and has a 7.2 h physical half-life, as an alternate radionuclide to ^{225}Ac for PSMA TAT. Studies with ^{211}At delivered by multiple targeting vectors have demonstrated its exquisite cytotoxicity at activity levels that result in little if any normal tissue toxicity [11]. Based on our extensive experience with its radioiodinated analogue [12], [^{211}At]DCABzL (Figure 1) was selected for proof of principle studies and shown to accumulate and be therapeutically effective in PSMA+ PC3 PIP xenografts [13]. Although encouraging responses also were observed in a challenging PC3-ML-Luc-PSMA micrometastatic model after treatment with a single dose [^{211}At]DCABzL, long term toxicity studies demonstrated significant late stage nephrotoxicity in CD1 mice, consistent with the high and prolonged renal accumulation of this agent.

In the current study, we have evaluated several next-generation ^{211}At-labeled PSMA inhibitors with the goal of identifying a compound with lower kidney uptake and good accumulation in PSMA-expressing PC3 PIP xenografts. Our strategy was to utilize structures based on two prosthetic groups – astatopyridinyl [14] and astatoguanidinomethyl benzoyl [15] – that exhibited good in vivo stability, low retention in the kidney as well as effective trapping in tumor xenografts when used for ^{211}At labeling of internalizing monoclonal antibodies and fragments. Except with one compound, biodistribution experiments were performed in paired-label format with each ^{131}I-labeled analogue to evaluate possible contribution of relatively low carbon-astatine bond strength on in vivo behavior.

2. Materials and Methods

2.1. General

Chemical reagents and solvents purchased from commercial sources were of analytical grade or better and used as such. Sodium [^{131}I]iodide [15–50 TBq (400–1350 Ci)/mmol] in 0.1 M NaOH was obtained from Perkin Elmer Life and Analytical Sciences (Boston, MA). Astatine-211 was produced on the Duke University CS-30 cyclotron *via* the ^{209}Bi(α, 2n)^{211}At reaction by bombarding natural bismuth metal targets with 28 MeV α-particles essentially as described previously [16, 17]. Compounds (((*S*)-1-carboxy-5-(4-[^{131}I]iodobenzamido)pentyl)carbamoyl)-L-glutamic acid ([^{131}I]DCIBzL) [12] and (((S)-1-carboxy-5-(4-[^{211}At]astinatobenzamido)pentyl)carbamoyl)-L-glutamic acid ([^{211}At]DCABzL) [13] were synthesized as reported. Bis(4-methoxybenzyl) (((*S*)-1-((4-methoxybenzyl)oxy)-1-oxo-6-(5-(tributylstannyl)nicotinamido)hexan-2-yl)carbamoyl)-L-glutamate (1), (((*S*)-1-carboxy-5-(5-iodonicotinamido)pentyl)carbamoyl)-L-glutamic acid (YC-550), bis(4-methoxybenzyl) (((*S*)-6-(5-[^{131}I]iodonicotinamido)-1-((4-methoxybenzyl)oxy)-1-oxohexan-2-yl)carbamoyl)-L-glutamate [^{131}I]**16**), and ((1-carboxy-5-(5-[^{131}I]iodonicotinamido)pentyl)carbamoyl)-L-glutamic acid ([^{131}I]YC-550) were synthesized as reported [12]. Compounds (**8**), 2,5-dioxopyrrolidin-1-yl 4-(guanidinomethyl)-3-(trimethylstannyl)benzoate (*N*-succinimidyl 3-((1, 2-bis(*tert*-butoxycarbonyl)guanidino)methyl)-5-(trimethylstannyl)benzoate; Boc_2-*iso*-SGMTB) and

2,5-dioxopyrrolidin-1-yl 4-((1,3-bis(*tert*-butoxycarbonyl)guanidino)methyl)-3-iodobenzoate (**9**) (*N*-succinimidyl 3-((1, 2-bis(*tert*-butoxycarbonyl)guanidino)methyl)-5-iodobenzoate; Boc_2-*iso*-SGMIB) were synthesized as reported [18]. (*S*)-*Tert*-butyl 2-amino-6-(((benzyloxy)carbonyl)amino)hexanoate hydrochloride (**11**), 2-(4-iodophenyl)ethan-1-amine (both from Merck KGaA, Darmstadt, Germany), and bis (2,5-dioxopyrrolidin-1-yl) octanedioate (Combi-Blocks, San Diego, CA) were purchased from commercial sources. All other reagents were purchased from Sigma-Aldrich (St. Louis, MO) except where noted. Flash chromatographic purification of synthesized compounds was performed either with the Biotage Isolera chromatography system (Charlotte, NC) using their pre-packed SNAP Ultra silica and C18 cartridges or manually using columns packed with silica gel (MP SiliTech 32–63 Silica Gel D 60 Å, purchased from Bodman, Aston, PA). Preparative thick layer chromatography was used for small-scale purification with plates obtained from Whatman (Clifton, NJ) or EM Science. High-performance liquid chromatography (HPLC) was performed using the following two systems: 1) for radiolabeled compounds: a Beckman Gold HPLC system equipped with a Model 126 programmable solvent module, a Model 166 NM variable wavelength detector, a Model 170 radioisotope detector and a Beckman System Gold remote interface module SS420X; data were acquired using 32 Karat® software (Beckman Coulter, Inc., Brea, CA). In later experiments, the gamma detector in this system was replaced with a ScanRam RadioTLC scanner/HPLC detector combination (LabLogic; Brandon, Fl) and ensuing radio-HPLC analyses were performed using this detector; 2) for analytical and semi-preparative HPLC of unlabeled compounds, a Waters Model Delta 600 semi-preparative system with a Model 600 controller and a Model 2487 dual wavelength absorbance detector; data were acquired using Millenium software. Reversed-phase HPLC was performed using a Waters 4.6 × 250-mm XTerra RP18 (5 μm) column and a 19 × 150 mm XTerra RP18 (7 μm) column for analytical and semi-preparative runs, respectively. Proton and ^{13}C NMR spectra were obtained on a Varian 400 or 500 MHz NMR spectrometer (Palo Alto, CA) or a Bruker Ultrashield 500 MHz spectrometer (Billerica, MA); chemical shifts are reported in δ units using the residual solvent peak as reference. Mass spectra were recorded on an Agilent LCMS-TOF with DART or a Bruker Daltonics Esquire 3000 Plus spectrometer. An automated gamma counter — either an LKB 1282 (Wallac, Finland) or a Perkin Elmer Wizard II (Shelton, CT) — and a CRC-7 dose calibrator (Capintec, Pittsburgh, PA) were used to measure lower and higher levels of radioactivity, respectively. For measuring ^{211}At activity, the ^{133}Xe setting in the CRC-7 dose calibrator was used and the values were multiplied by a previously established correction factor of 2.3.

2.2. Synthesis of unlabeled compounds

2.2.1. Di-tert-butyl (((S)-1-(tert-butoxy)-1,5-dioxo-5-((4-(tri-n-butylstannyl)phenethyl)amino)pentan-2-yl)carbamoyl)-L-glutamate (2)—

A mixture of 5-(*tert*-butoxy)-4-(3-((*S*)-1,5-di-*tert*-butoxy-1,5-dioxopentan-2-yl)ureido)-5-oxopentanoic acid (**5**) [19] (0.10 g, 0.20 mmol), TSTU (0.07 g, 0.22 mmol) and DIPEA (0.05 g, 0.41 mmol) in DMF (1 mL) was stirred at room temperature for 5 h. A solution of 2-(4-(tributylstannyl)phenyl)ethan-1-amine [20] (0.08 g, 0.20 mmol) in DMF (1 mL) was added dropwise to the above. The reaction mixture was stirred overnight, concentrated and purified by silica gel flash chromatography eluted with 35% EtOAc/ hexanes, providing 0.07 g (37%) of an oily material: ^1H NMR (500 MHz, $CDCl_3$) δ_H 7.41 (d, $J = 10$ Hz, 2H), 7.20

(d, J = 5 Hz, 2H), 6.59 (m, 1H), 5.36–5.30 (m, 2H), 4.33 (m, 2H), 4.15 (m, 1H), 3.52–3.49 (m, 2H), 2.83–2.80 (m, 2H), 2.37– 2.10 (m, 5H), 1.97–1.86 (m, 2H), 1.71–1.54 (m, 2H), 1.47 (m, 27H), 1.39–1.27 (m, 10H), 1.07–1.04 (m, 6H), 0.90 (m, 9H). ESI MS *m/z:* 880.4 $(M + H)^+$, 904.3 $(M + Na)^+$.

2.2.2. Di-tert-butyl (((S)-1-(tert-butoxy)-5-((4-iodophenethyl)amino)-1,5-dioxopentan-2yl)-carbamoyl)-L-glutamate (6)—This reaction was performed essentially as above by substituting *para*-5-iodophenethlamine (0.06 g, 0.20 mmol) for 2-(4-(tributylstannyl)phenyl)ethan-1-amine. The reaction mixture was stirred overnight, concentrated and purified by C-18 flash column chromatography using a 30 g Biotage SNAP Ultra C18 Cartridge eluted with 70–100% acetonitrile/ H_2O, providing 0.14 g (95%) of an oil: ^{1}H NMR (500 MHz, $CDCl_3$) δ_H 7.57 (d, J = 10 Hz, 2H), 7.37 (bs, 1 H), 6.94 (d, J = 10 Hz, 2H), 5.89–5.80 (m, 2H), 4.27–4.18 (m, 2H), 10 3.49–3.40 (m, 2H), 2.75 (t, J = 5 Hz, 2H), 2.39–2.21 (m, 2H), 2.07–2.05 (m, 2H), 1.87–1.75 (m, 2H), 1.42 (m, 27H); ESI MS *m/z:* 718.2 $(M+H)^+$.

2.2.3. (((S)-1-Carboxy-4-((4-iodophenethyl)amino)-4-oxobutyl)carbamoyl)-L-glutamic acid (HS-549)—A cold solution of 50% TFA in dichloromethane (2 mL) was added to di-*tert*-butyl (((*S*)-1-(*tert*-butoxy)-5-((4-iodophenethyl)amino)-1,5-dioxopentan-2-yl)carbamoyl)-L-glutamate (**6**; 0.14 g, 0.19 mmol) and the solution stirred at room temperature for 2 h. The reaction mixture was concentrated and purified by C-18 flash column chromatography using a 30 g Biotage SNAP Ultra C18 Cartridge eluted with 70–90% MeOH/water. Lyophilization of chromatographic fractions containing the desired product provided 0.07 g (62%) of a yellowish semisolid: ^{1}H NMR (500 MHz, 1:1 CD_3CN:D_2O) δ_H 8.11 (d, J = 5 Hz, 2H), 7.50 (d, J = 5 Hz, 2H), 4.68–4.67 20 (m, 1H), 4.61–4.59 (m, 1H), 3.82–3.79 (m, 2H), 3.19–3.16 (m, 2H), 2.88 (t, J = 5 Hz, 2H), 2.68–2.65 (m, 2H), 2.57–2.54 (m, 1H), 2.46 (m, 2H), 2.37–2.27 (m, 2H); ^{13}C NMR (125 MHz, 1:1 CD_3CN:D_2O) δ ppm 177.0, 176.3, 174.9, 159.5, 140.2, 138.4, 132.1, 119.5, 91.9, 53.5, 53.3, 41.2, 35.2, 33.0, 30.9, 28.7, 27.6. ESI MS *m/z*: 550.0 $(M + H)^+$.

2.2.4. (S)-Di-tert-butyl 2-(3-((S)-6-(4-((1,3-bis(tert-butoxycarbonyl)guanidino)methyl)-3-(trimethylstannyl)benzamido)-1-(tert-butoxy)-1-oxohexan-2-yl)ureido)pentanedioate (3)—Triethylamine (39.3 mg, 0.21 mmol) was added to a solution of (*S*)-di-*tert*-butyl 2-(3-((*S*)-6-amino-1-(*tert*-butoxy)-1-oxohexan-2-yl)ureido)pentanedioate (**7**) [21, 22] (20mg, 0.04 mmol) and Boc_2-SGMTB (**8**) [18] (26.8 mg, 0.04 mmol) in 20 mL of dichloromethane kept at 5–10°C. The reaction was allowed to proceed at room temperature for 16 h and 15 mL water was added. The organic layer was separated, dried with anhydrous sodium sulfate, and dichloromethane was evaporated. The crude material was subjected to preparative thick layer chromatography using 1:1 hexanes:ethyl acetate as the mobile phase to obtain 30 mg (0.03 mmol, 71.3% yield) of **3** as a foam: ^{1}H-NMR (400 MHz, $CDCl_3$) δ_H 9.56–9.30 (bs, 2H), 7.80 (s, 1H), 7.70–7.65 (d, J = 8.4 Hz, 1H), 7.03–6.99 (d, J = 8.4 Hz, 1H), 6.55–6.50 (dd, 1H), 5.27–5.18 (m, 4H), 4.37–4.28 (m, 2H), 3.47–3.40 (m, 2H), 2.47–2.00 (m, 3H), 1.90–1.10 (m, 52H), 0.10 (s, 9H). HRMS: Calcd for $C_{46}H_{79}N_6O_{12}Sn$ $(M+H)^+$: 1027.4778; Found: 1027.4784.

2.2.5. (S)-Di-tert-butyl 2-(3-((S)-6-(4-((1,3-bis(tert-butoxycarbonyl)guanidino)methyl)-3-iodobenzamido)-1-(tert-butoxy)-1-oxohexan-2-yl)ureido)pentanedioate (10)—The synthesis of **10** was performed essentially as for **3** at the same scale but replacing Boc_2-SGMTB with Boc_2-SGMIB. The crude material was subjected to preparative thick layer chromatography using 1:1 hexanes:ethyl acetate as the mobile phase to obtain 28mg (0.03 mmol, 69.0% yield) of **10** as an off white solid: ^{1}H-NMR (400 MHz, $CDCl_3$) δ_H 9.50–9.30 (bs, 2H), 8.28 (s, 1H), 7.80 (d, J = 8.4 Hz, 1H), 7.00 (d, J = 8.4 Hz, 1H), 6.85–6.70 (m, 1H), 5.25–5.18 (m, 3H), 4.37–4.27 (m, 2H), 3.47–3.33 (m, 2H), 2.47–2.00 (m, 3H), 2.40–1.22 (m, 53H). HRMS: Calcd for $C_{43}H_{70}IN_6O_{12}$ $(M+H)^+$: 989.4096; Found: 989.4082.

2.2.6. Amino((4-((5-carboxy-5-(3-(1,3-dicarboxypropyl)ureido)pentyl)carbamoyl)-2-iodobenzyl)amino)methaniminium (GV-620)—Trifluoroacetic acid (5 mL) was added to **10** (25 mg, 0.025 mmol). The mixture was stirred at room temperature for 17 h, trifluoroacetic evaporated, and the residue dried to obtain 15 mg (0.024 mmol of TFA salt, 81% yield) of GV-620. The crude product was purified by reversed-phase chromatography eluting a Biotage Sfär C18 6-g cartridge with 9:1 H_2O:MeCN to 100% MeCN over 30 min at 6 mL/min). ^{1}H-NMR (500 MHz, CD_3OD) δ_H 8.27 (s, 1H), 7.82 (d, J = 8.4 Hz, 1H), 7.40 (d, J = 8.4 Hz, , 1H), 4.41 (s, 2H), 4.22 (m, 2H), 3.24 (m, 2H), 2.29 (m, 2H), 2.10 (m, 1H), 1.84 (m, 2H), 1.61 (m, 3H), 1.42 (m, 2H); ^{13}C NMR (125 MHz, CD_3OD) δ ppm 176.9, 176.3, 168.2, 160.5, 159.2, 143.3, 140.1, 137.4, 129.4, 129.0, 99.2, 74.2, 64.7, 54.3, 51.4, 41.2, 33.6, 31.0, 30.2, 29.3, 24.4. LRMS: 621.1 $(M+H)^+$. HRMS: Calcd for $C_{21}H_{30}IN_6O_8$ $(M+H)^+$: 621.1170; Found: 620.1180.

2.2.7. 2,5-Dioxopyrrolidin-1-yl (S)-8-((6-(((benzyloxy)carbonyl)amino)-1-(tert-butoxy)-1-oxohexan-2-yl)amino)-8-oxooctanoate (12)—A solution of (*S*)-*tert*-butyl 2-amino-6-(((benzyloxy)carbonyl)amino)hexanoate hydrochloride (**11**; 1.01 g, 2.71 mmol) in acetonitrile (50 mL) was added over a period of 30 min to a solution of disuccinimidyl suberate (1 g, 2.71 mmol) and triethylamine (0.38 mL, 2.71 mmol) in acetonitrile (50 mL), and the mixture was stirred at room temperature for 4 h. Acetonitrile was evaporated to reduce the volume to half, and the remaining mixture was partitioned between water and ethyl acetate. The pooled ethyl acetate solution was dried with anhydrous sodium sulfate, filtered and concentrated. The crude product was purified using a Biotage 25 g SNAP ULTRA column and 7:3 hexanes:ethyl acetate as the mobile phase to yield 1 g (1.70 mmol; 62.5%) of **12** as a white solid: ^{1}H-NMR (400 MHz, $CDCl_3$) δ_H 7.38 – 7.25 (m, 5H), 6.17–6.08 (d, J = 7.8 Hz,1H), 5.06 (m, 3H), 4.95–4.87 (bs, 1H), 4.51–4.45 (m, 1H), 3.38–3.30 (m, 1H), 3.32–3.04 (m, 4H), 2.86–2.72 (m, 6H), 2.62–2.52 (m, 3H), 2.19 (t, J = 8.0 Hz, 2H), 1.81–1.06 (m, 16H). LRMS: 590.3 (M^+), 612.3 $(M+Na)^+$. HRMS: Calcd for $C_{30}H_{44}N_3O_9$ $(M+H)^+$: 590.3078; Found: 590.3067.

2.2.8. Tetra-tert-butyl (9S,24S,28S)-3,11,18,26-tetraoxo-1-phenyl-2-oxa-4,10,19,25,27-pentaazatriacontane-9,24,28,30-tetracarboxylate (13)—Triethylamine (0.17 mL) was added to a solution of **7** [21, 22] (0.5 g, 1.03 mmol) and **12** (0.61 g, 1.03 mmol) in acetonitrile (40 mL) kept at 5–10°C. After 2 h, the reaction mixture

was partitioned between water and ethyl acetate. The pooled ethyl acetate solution was dried with anhydrous magnesium sulfate and concentrated. The residue was purified using a Biotage 25 g SNAP ULTRA column and 5:1 hexanes:ethyl acetate as the mobile phase to yield 0.77 g (0.80 mmol; 78%) of **13** as a white foam: ^{1}H-NMR (400 MHz, $CDCl_3$) δ_H 7.38 – 7.25 (m, 5H), 6.17–6.08 (d, *J =7.6 Hz,* 1H), 5.06 (m, 3H), 4.95–4.87 (bs, 1H), 4.55–4.46 (m, 2H), 3.22–3.16 (m, 4H), 2.22–2.16 (m, 4H), 1.85–1.24 (m, 63H). LRMS: 963 $(M+H)^+$; HRMS: Calcd for $C_{50}H_{84}N_5O_{13}$ $(M+H)^+$: 962.6066; Found: 962.6064.

2.2.9. Tetra-tert-butyl (3S,7S,22S)-26-amino-5,13,20-trioxo-4,6,12,21-tetraazahexacosane-1,3,7,22-tetracarboxylate (14)—Ammonium formate (0.46 g, 7.27 mmol) and **13** (0.70 g, 0.73 mmol) were dissolved in ethanol (25 mL) and the solution was degassed. Palladium on carbon (0.1 g, 0.94 mmol) was added and the solution degassed again. Hydrogen was introduced to the flask and the mixture was stirred under a hydrogen atmosphere for 16 h. The solution was degassed and the flask was purged with argon. The mixture was filtered over a Celite-545 bed, and the bed was washed with 50 mL of ethanol. The filtrate was concentrated to dryness, the residue taken in dichloromethane and the mixture filtered through Celite to remove any insolubles. The filtrate was concentrated to dryness to give 0.47 g (0.57 mmol, 78%) of **14** as a foam. ^{1}H-NMR (400 MHz, $CDCl_3$) δ_H 8.52 (bs, 1H), 7.30 (d, 1H, *J=7.80*), 6.88 (bs, 1H), 6.50 (bs, 1H), 6.40 (bs, 1H), 4.45–4.20 (m, 4H), 3.50–2.95 (m, 4H), 2.65 1.85–1.30 (m, 64H) LRMS: = 829 $(M+H)^+$.LRMS: = 829 $(M+H)^+$. LRMS: = 829 $(M+H)^+$. HRMS: Calcd for $C_{42}H_{78}N_5O_{11}$ $(M+H)^+$: 828.5698; Found: 828.5700.

2.2.10. Tetra-tert-butyl (7S,22S,26S)-1-(4-(((Z)-1,2-bis(tert-butoxycarbonyl)guanidino)methyl)-3-(trimethylstannyl)phenyl)-1,9,16,24-tetraoxo-2,8,17,23,25-pentaazaoctacosane-7,22,26,28tetracarboxylate (4)—The synthesis of **4** was performed similar to that **3** and **10** using triethylamine (5.12 μL), **14** (57 mg, 0.07 mmol) Boc_2-SGMTB (30 mg, 0.05 mmol) and dichloromethane (15 mL). The crude product was subjected to preparative thin layer chromatography using 1:1 hexanes:ethyl acetate to yield 40 mg (0.03 mmol, 63.8% yield) of **4** as a tan solid: ^{1}HMR (400 MHz, $CDCl_3$) δ_H 9.50–9.25 (bs , 2H), 7.88 (s, 1H), 7.62 (d, *J* = 8.4 Hz, 1H), 6.95 (d, *J* = 8.4 Hz, 1H), 6.70–6.65 (t, *J* = 7.6 Hz, 1H), 6.42–6.33 (m, 2H), 5.66–5.60 (d, *J* = 8.6 Hz, 1H), 5.55–5.50 (d, *J* = 8.6 Hz,1H), 5.22 (s, 2H), 4.52–4.45 (m, 1H), 4.33–4.23 (m, 2H), 3.62 (s, 1H), 3.45–3.31 (m, 2H), 3.28–3.18 (m, 1H), 3.13–3.05 (m, 1H), 2.32–1.08 (m, 82H), 0.36 (s, 9H). LRMS: Cluster peaks at 1367.8 $(M+H)^+$. HRMS: Calcd for $C_{64}H_{111}N_8O_{16}Sn$ $(M+H)^+$: 1367. 7140; Found: 1367.7147.

2.2.11. Tetra-tert-butyl (7S,22S,26S)-1-(4-(((Z)-1,2-bis(tert-butoxycarbonyl)guanidino)methyl)-3-iodophenyl)-1,9,16,24-tetraoxo-2,8,17,23,25-pentaazaoctacosane-7,22,26,28-tetracarboxylate (15)— Compound **15** was synthesized essentially as **4** using triethylamine (6.78 μL), **14** (50.4 mg, 0.06 mmol), Boc_2-SGMIB (25 mg, 0.04 mmol) and 15 mL dichloromethane. The crude material was subjected to thick layer chromatography using hexanes and ethyl acetate (1:1) to give 30 mg (0.023 mmol, 55.6% yield) of ***15*** as a tan solid: ^{1}H-NMR (400 MHz, $CDCl_3$) δ_H 9.58–9.35 (bs, 2H), 8.36 (s, 1H), 7.81 (d, *J* = 8.4 Hz, 2H), 7.05 (m,1H)6.98 (d, *J* = 8.4

Hz, 2H), 6.44 (m, *J* = 8.6, 2H), 6.31 (m, 1H), 5.63 (m, *J=8.6,* 2H), 5.56 (d, *J=8.6,* 2H*),* 5.20 (s, 2H), 4.58–4.52 (m, 1H), 4.38–4.28 (m, 2H), 3.52–3.13 (m, 4H), 2.36–2.05 (m, 8H), 1.92–1.27 (m, 73H). LRMS: 1329.6 $(M+H)^+$, 1351.6 $(M+Na)^+$. HRMS: Calcd for $C_{61}H_{102}IN_8O_{16}$ $(M+H)^+$: 1329.6458; Found: 1329.6456.

2.2.12. Amino((4-(((3S,7S,22S)-22-(tert-butoxycarbonyl)-1,3,7-tricarboxy-5,13,20-trioxo-4,6,12,21-tetraazahexacosan-26-yl)carbamoyl)-2-iodobenzyl)amino)methaniminium (GV-904)—

Trifluoroacetic acid (5mL) was added to **15** (56 mg, 0.04 mmol). The mixture was stirred at 20°C for 17 h, trifluoroacetic was evaporated and the residue dried to obtain 40 mg (0.04 mmol of TFA salt, 94% yield) of GV-904 as an oil. The crude product was purified by reversed-phase chromatography eluting a Biotage® Sfär C18 6-g cartridge with 100% H_2O for 5 min, then 9:1 H_2O:MeCN to 100% MeCN over 30 min at 6 mL/min. ^{1}H-NMR (500 MHz, CD_3OD) δ_H 8.37 (s, 1H), 7.86 (m, 1H), 7.40 (d, *J = 8.4,* 1H), 4.52–4.18 (m, 4H), 3.44–3.08 (m, 4H), 2.44–2.22 (m, 6H), 1.96–1.18 (m, 34H); ^{13}C NMR (125 MHz, CD_3OD) δ ppm 176.9, 176.7, 176.6, 168.1, 160.5, 159.3, 143.3, 140.1, 139.0, 137.4, 130.3, 129.5, 129.4, 129.0, 126.6, 99.2, 74.2, 64.8, 54.4, 54.0, 53.8, 51.4, 41.1, 40.5, 37.4, 33.6, 32.3, 31.6, 30.1, 29.7, 27.2, 27.1, 24.5, 24.3, 21.8. LRMS: 905.3 $(M+H)^+$. HRMS: Calcd for $C_{35}H_{54}IN_8O_{12}$ $(M+H)^+$: 905.2906; Found: 905.2897.

2.3. Radiochemistry

2.3.1. Radioiodination—

Synthesis of novel radioiodinated compounds was performed utilizing the following general conditions with slight variations as noted. Iodine-131 (1 – 3 μL; 60–75 MBq), a solution of NCS in methanol (100 μL of 1 mg/mL) and acetic acid (20 μL) were added to 50 μg of the respective tin precursor **2** (57 nmol), **3** (49 nmol) or **4** (37 nmol). The vial was vortexed and the reaction allowed to proceed at 20°C for 10 min (20 min for **2**) to produce intermediates **18**, **20** and **22**, respectively. Methanol and other volatiles was evaporated with a gentle stream of argon and subsequently, addition of 50 μL of ethyl acetate and its evaporation was performed thrice. TFA (200 μL) or, for **18**, a solution of anisole in TFA (3%, 100 μL) was added, and the mixture left at 20°C for 20 min (30 min for **18**). TFA was evaporated with an argon stream and to insure complete removal of TFA, 50 μL of ethyl acetate was added and then evaporated thrice. The residual activity was reconstituted in 50 μL of a 1:9 acetonitrile:water mixture and injected onto a reversed-phase HPLC column (Waters XTerra; RP18, 4.6 × 250 mm, 5 μm). The column was eluted at flow rate of 1 mL/min with a gradient consisting of 0.1% TFA each in water (A) and acetonitrile (B); the proportion of B was kept at 10% for 5 min and then increased linearly to 100% over 30 min. Under these conditions, t_R of [^{131}I]HS-549, [^{131}I]GV-620 and [^{131}I]GV-904 was about 20 min, 18 min and 18–19 min, respectively. Some batches of [^{131}I]HS-549 was also purified using a Phenomenix Luna C18, 10 × 250 mm, 10 μm column with isocratic elution using 25% acetonitrile in water with 0.1% TFA at a flow of 4 mL/min (t_R = 18 min). The pooled HPLC fractions containing the product were evaporated with an argon stream to remove most of the acetonitrile, diluted with water to 10 mL, and gently passed through an activated C18 SepPak cartridge (Waters); in some batches of [^{131}I]HS-549 an Oasis HLB light cartridge was used. The cartridge was washed with 2 × 5 mL water and the product was

eluted with 0.25 mL portions of ethanol. Portions 2–5 containing most of the activity were pooled, ethanol evaporated and the activity was reconstituted in PBS.

2.3.2. Astatine-211 labeling—As with radioiodinated compounds, the following general procedure with slight variations was used for the synthesis of ^{211}At-labeled analogues. A solution of ^{211}At (30 – 238 MBq) in a 1 mg/mL solution of NCS in methanol (0.1 or 0.5 mL) [13] was added to 50 μg of the respective tin precursor **1** (47 nmol), **2** (57 nmol), **3** (49 nmol) or **4** (37 nmol). The solution was mixed by vortexing and incubated at 20°C (70°C for **1**) for 10 min to produce intermediates **17**, **19**, **21** and **23**, respectively. Methanol was evaporated with a gentle stream of argon and in some cases to insure complete removal of methanol, addition of 50 μL of ethyl acetate and its evaporation was performed thrice. A solution of anisole in TFA (3%; μL) was added and the mixture was allowed to react at 20°C for 30 min. Methanol was evaporated with a gentle stream of argon and a solution of anisole in TFA (3%; 100 μL) was added and the mixture incubated at 20°C for 30 min. TFA was evaporated with a gentle stream of argon, and to ensure complete removal of TFA, addition of 50 μL ethyl acetate and evaporation was performed thrice. The activity was taken in 50 μL of 9:1 water:acetonitrile and injected onto a reversed-phase column (Waters XTerra; RP18, 4.6 × 250 mm, 5 μm). The column was eluted at flow rate of 1 mL/min with a gradient consisting of 0.1% TFA each in water (A) and acetonitrile (B); the proportion of B was kept at 10% for 5 min and then increased linearly to 100% in 30 min. The retention time of [^{211}At]YC-550, [^{211}At]HS-549, [^{211}At]GV-620 and [^{211}At]GV-904 under these conditions was about 18–19 min, 21 min, 19–20 min and 18–19 min, respectively. The pooled HPLC fractions containing the product were evaporated with an argon stream to remove most of the acetonitrile, diluted with water to 10 mL, and gently passed through an activated C18 SepPak cartridge (Waters). The cartridge was washed with 2 × 5 mL water and the product was eluted with 0.25 mL portions of ethanol. Portions containing the product (typically 2–5) were pooled, ethanol evaporated, and the residual activity reconstituted with PBS.

2.4. Cell lines and mouse models

PSMA+ PC3 PIP cells (human metastatic [bone] prostate carcinoma) engineered to express PSMA stably and PSMA- PC3 flu cells were a generous gift by Warren Heston (Cleveland Clinic). These cells were cultured in T175 flasks using RPMI 1640 medium (Sigma) supplemented with 10% FBS and penicillin/streptomycin (100 U/mL/100 μg/mL) at 37 °C in 5% CO_2 in air. When a sufficient number of cells were present in culture, the cells were trypsinized and formulated in sterile Hanks buffered saline solution (Sigma, HBSS) and counted using a hemocytometer and trypan blue dye to confirm cell viability. All animal studies were performed following protocols approved by the Institutional Animal Care and Use Committee of Johns Hopkins University and Duke University. Both athymic nu/nu and severe combined immunodeficient (SCID) male mice weighing 20–25 g were used in this study. Typically, 2–5 × 10^6 cells were injected subcutaneously such that PC3 PIP cells were injected behind the left shoulder and PC3 flu cells were injected behind the right shoulder of the mice. Biodistribution was performed when the tumors reached 3–7 mm in diameter.

2.5. PSMA inhibition assay

The PSMA inhibitory ability of novel agents, along with that of ZJ43 [23] as a positive control, was determined by a fluorescence-based assay as reported [24]. Briefly, LNCaP cell extracts (25 μL) were incubated with various amounts of the inhibitor (12.5 μL) in the presence of 4 μM *N*-acetylaspartylglutamate (NAAG; 12.5 μL) for 120 min. The amount of glutamate released upon hydrolysis of NAAG was measured by incubation with a working solution (50 μL) of the Amplex Red Glutamic Acid Kit (Life Technologies, Grand Island, NY) for 60 min. Fluorescence was measured with a VICTOR3V multilabel plate reader (Perkin Elmer Inc., Waltham, MA) with excitation at 530 nm and emission at 560 nm. Fluorescence intensity was plotted against log[M] and from this IC_{50} values were obtained as the concentration at which enzyme activity was inhibited by 50%. Assays were performed in triplicate. Enzyme inhibitory constants (*K*i values) were calculated using the Cheng-Prusoff equation [25]. Data analysis was performed using GraphPad Prism version 4.00 for Windows (GraphPad Software, San Diego, CA).

2.6. Biodistribution

Several paired label biodistribution studies were performed in this work comparing the ^{131}I-labeled and ^{211}At-labeled analogues of the same novel molecule. In general, mice were injected with the radiolabeled pairs via tail vein, and at indicated time points, samples of blood and urine were collected and the mice killed by an overdose of isofluorane. Tumor and tissues of interest were harvested, blot-dried, weighed and counted in an automated gamma counter for ^{131}I and ^{211}At activity. From these, the percentage of injected dose (%ID) per organ, ID per gram of tissue (%ID/g), and tumor-to-tissue ratios (TTR) were calculated. The details (mouse strain, radiotracers, injected dose, and time points) of various biodistribution studies performed are as follows: 1) Athymic, [^{211}At]YC-550 (148 kBq) vs [^{131}I]DCIBzL (185 kBq) with time points of 1 h, 2 h, 4 h and 21 h. 2) SCID, [^{211}At]HS-549 (185 kBq) and [^{131}I]HS-549 (185 kBq) with time points of 1 h, 2 h and 21 h. 3) SCID, [^{211}At]GV-620 (185 kBq) and [^{131}I]GV-620 (185 kBq) with time points of 1 h, 2 h, 4 h, 14 h and 21 h. 4) SCID, [^{211}At]GV-904 (185 kBq) and [^{131}I]GV-904 (185 kBq) with time points of 1 h, 2 h, and 21 h.

2.7. Statistical analyses

Values are reported as mean ± SD. The statistical significance of differences in uptake between the two radiotracers that were co-incubated with cells or co-administered in mice was determined by a 2-tailed, paired Student's t-test using Excel; a *P*-value of <0.05 was considered to be significant.

3. Results

3.1. Chemistry

The structures of DCIBzL [12], DCABzL [13] and those of the novel compounds investigated in this work are presented in Fig. 1. As shown in Scheme 1, the protected standard (**6**) and tin precursor (**2**) of HS-549 were synthesized by the TSTU-mediated conjugation of 5-(*tert*-butoxy)-4-(3-((*S*)-1,5-di-*tert*-butoxy-1,5-dioxopentan-2-yl)ureido)-5-

oxopentanoic acid (**5**) [19] with 4-iodophenethylamine and 4-tri(n-butyl)stannyl phenethylamine [20] in 95% and 37% yield, respectively. TFA-mediated deprotection of (**6**) rendered the HS-549 standard in 62% yield (Fig. S1). The protected standard (**10**) and the tin precursor (**3**) of GV-620 were synthesized by the conjugation of the basic pharmacophore molecule, (*S*)-di-*tert*-butyl 2-(3-((*S*)-6-amino-1-(*tert*-butoxy)-1-oxohexan-2-yl)ureido)pentanedioate (**7**), with 2,5-dioxopyrrolidin-1-yl 4-((1,2-bis(*tert*-butoxycarbonyl)guanidino)methyl)-3-iodobenzoate (Boc_2-SGMIB; **9**) or 2,5-dioxopyrrolidin-1-yl 4-((1,2-bis(*tert*-butoxycarbonyl)guanidino)methyl)-3-(trimethylstannyl)benzoate (Boc_2-SGMTB; **8**), in 69% and 71% yield, respectively (Scheme 2). The final deprotected standard of GV-620 was obtained in 81% yield by treatment with TFA (Fig. S2). The steps for the synthesis of protected standard (**15**), tin precursor (**4**) and final standard of GV-904 are shown Scheme 3. The intermediate **12** was obtained by the conjugation of commercially available compound **11** with disuccinimidyl suberate in 63% yield and its treatment with **7** delivered **13** in 78% yield. Deprotection of the CbZ group (78% yield) and conjugation of the resultant intermediate **14** with Boc_2-SGMIB provided the protected standard of GV-904 (**15**) in 56% yield, which on treatment with TFA gave the final standard of GV-904 (94%; Fig. S3). The tin precursor **4** was obtained in 78% yield by the conjugation of **14** Boc_2-SGMTB. NMR and mass spectral data for all new compounds are consistent with their structures.

3.2. PSMA inhibition

The IC_{50} values obtained from the Amplex assay for HS-549, GV-620 and GV-904 were 0.43 nM, 2.24 nM, and 0.88 nM, respectively (Fig. S4–S6). The corresponding *K*i values – 0.09 nM, and 0.45 nM, and 0.18 nM, respectively - were similar to those obtained for other PSMA inhibitors [26].

3.3. Radiochemistry

3.3.1. Radioiodination—Although performed only once, [^{131}I]HS-549 was synthesized in 91% radiochemical yield (RCY) and 99% radiochemical purity (RCP; Fig. S7); the ^{125}I analogue was synthesized in 78 ± 10% RCY (n = 3) and 98 ± 2% RCP. The RCY for the synthesis of [^{131}I]GV-620 was 78 ± 3% (n = 6) and the RCP was 96 ± 5% (Fig. S8). Iodine-131-labeled GV-904 was synthesized with an RCY of 73 ± 4% (n = 6) and with an RCP of 99 ± 1% (Fig. S9).

3.3.2. Astatination—The tin precursor **1** was labeled with ^{211}At to obtain [^{211}At]YC-550 in 32 ± 26% RCY (n = 3) and RCP was 91 ± 8% (Fig. S10). The t_R of the iodo standard is slightly higher than that of [^{211}At]YC-550, an observation that has been reported before for 4-iodo- and 4-[^{211}At]astatophenylalanine [27]. The RCY for the synthesis of [^{211}At]HS-549, performed twice, was 53% and 79% with a RCP of 90% and 99% (Fig. S11). [^{211}At]GV-620 was synthesized twice in a RCY of 54% and 77% with a RCP of 91% and 95% (Fig. S12). Finally, [^{211}At]GV-904 was synthesized in a RCY of 52 ± 12% (n = 7) and with a RCP of 92 ± 4% (Fig. S13).

3.4. Biodistribution

Complete biodistribution data sets for all the ^{211}At- and ^{131}I-labeled PSMA inhibitors are presented in Tables 1–4 with the most salient *in vivo* results provided in Figures 2–7 and summarized below. As shown in Fig. 2A, [^{211}At]HS-549 demonstrated the highest uptake in PSMA+ PC-3 PIP xenografts (SCID model) at early time points (43.3 ± 9.8% ID/g and 42.1 ± 7.2% ID/g at 1 h and 2 h, respectively); however, its tumor levels decreased considerably by 21 h (10.6 ± 9.9% ID/g). With the caveat that [^{211}At]YC-550 was evaluated in an athymic mouse model, the next two best compounds with respect to PSMA+ PC-3 PIP xenograft uptake were [^{211}At]GV-904 (12–23% ID/g) and [^{211}At]GV-620 (14–18% ID/g). While the uptake of [^{211}At]DCABzL in PSMA+ PC-3 PIP xenografts increased at 18 h [13], in contrast, a decrease was seen at the 21 h time point for all the novel ^{211}At-labeled compounds. Uptake for all new ^{211}At-labeled compounds in PSMA- PC-3 flu xenografts was 11% or less of the level seen in PSMA+ PC-3 PIP xenografts. In general, radioiodinated compounds had a higher tumor uptake - in some cases 2-fold - than the corresponding ^{211}At-labeled derivative (Fig. 2B; $P < 0.05$ in most cases). As was the case with the ^{211}At-labeled analogues, all ^{131}I-labeled compounds demonstrated high uptake in PSMA+ PC-3 PIP xenografts with insignificant uptake in PSMA-PC-3 flu tumors. The uptake pattern of [^{131}I]GV-620 and [^{131}I]GV-904 in PSMA+ PC-3 PIP xenografts was similar to that seen for [^{131}I]DCIBzL [13]. On the other hand, uptake of [^{131}I]HS-549 in PSMA+ PC-3 PIP xenografts was more than two-fold higher than that for other radioiodinated compounds at 1 h and 2 h. For example, [^{131}I]HS-549 uptake at 1 h was 78.2 ± 19.1% ID/g compared with 24.3 ± 7.5% ID/g and 27.6 ± 7.5% ID/g for [^{131}I]GV-620 and [^{131}I]GV-904, respectively. The data above for [^{131}I]HS-549, [^{131}I]GV-620 and [^{131}I]GV-904 were obtained from paired label biodistributions of the radioiodinated and ^{211}At-labeled analogues performed using SCID mice; uptake at 1 h reported for [^{131}I]DCIBzL from a biodistribution in athymic mice was 19.0 ± 6.1% ID/g [13]. Contrary to that observed with [^{131}I]DCIBzL and similar to that seen for ^{211}At-labeled analogues, the tumor uptake of all new radioiodinated compounds decreased at 21 h, precipitously so for [^{131}I]HS-549, such that there was no delivery advantage compared with the other radioiodinated analogues at this time point.

Among ^{211}At-labeled analogues, [^{211}At]HS-549 displayed the lowest kidney activity levels (Fig. 3) with values of 46.7 ± 8.2% ID/g, 40.4 ± 15.5% ID/g and 2.6 ± 0.8% ID/g at 1 h, 2 h, and 21 h, respectively, while [^{211}At]YC-550 had the highest (135.3 ± 18.9% ID/g at 1 h). Notably, kidney activity levels for [^{211}At]YC-550 and other astatinated analogues were <10% by 21 h; in contrast, kidney activity for [^{211}At]DCABzL did not decrease much at 21 h. Renal clearance for the radioiodinated analogues was similar to that for the corresponding ^{211}At-labeled compound; however, kidney uptake of ^{131}I generally was higher than observed for co-administered ^{211}At. For the ^{131}I-labeled analogues (Fig.4), [^{131}I]HS-549 had the lowest kidney activity levels with values of 106 ± 18.9% ID/g, 96.6 ± 39.1% ID/g and 3.13 ± 1.65% ID/g at 1 h, 2 h, and 21 h, respectively, which were significantly higher ($P < 0.05$) than those noted above for co-administered [^{211}At]HS-549 at 1 and 2 h.

Uptake of [^{211}At]YC-550 in liver was comparable to that seen earlier for [^{211}At]DCABzL but all other novel ^{211}At-labeled derivatives had much higher liver uptake. At early time points, uptake in small intestine for all compounds was less than 6% ID/g except for

[^{211}At]GV-904. Uptake of all novel ^{211}At-labeled compounds in spleen was less than that observed for our first-generation compound [^{211}At]DCABzL. Even at 1 h, activity in blood from [^{211}At]GV-620 and [^{211}At]GV-904 was <1% ID/g. On the other hand, [^{211}At]HS-549 had 5.5 ± 0.8% ID/g and 2.8 ± 0.4% ID/g at 1 h and 2 h, respectively. The pyridine analogue [^{211}At]YC-550 displayed intermediate blood values. [^{211}At]HS-549 also demonstrated high uptake in lungs with 9.7 ± 1.3% ID/g, 8.2 ± 1.3% ID/g and 4.3 ± 0.7% ID/g at 1 h, 2 h and 21 h, respectively. As in blood, [^{211}At]GV-620 and [^{211}At]GV-904 had considerably lower levels in lungs and [^{211}At]YC-550 had intermediate values.

Renal activity levels for all radioiodinated analogues (Fig. 4) were more or less similar to those seen for [^{131}I]DCIBzL [13] at early time points (~100% ID/g) with the exception of [^{131}I]GV-620 at 1 h (169.7 ± 39.9% ID/g). However, unlike [^{131}I]DCIBzL, at 18–21 h, renal activity levels for the novel agents decreased considerably by 21 h. While the hepatic uptake of [^{131}I]GV-904 and [^{131}I]GV-620 was similar to that seen for their ^{211}At-labeled analogues {$P > 0.05$ at 1, 2 and 4 h (GV-620)}, with [^{131}I]HS-549 liver levels at 1 h and 2 h were about 3–6-fold higher ($P < 0.05$) than co-administered [^{211}At]HS-549. Uptake of [^{131}I]HS-549, [^{131}I]GV-620, and [^{131}I]GV-904 in small intestine and spleen was similar to that seen for their ^{211}At-labeled analogues. As observed with the ^{211}At-labeled analogues, [^{131}I]HS-549 had considerably higher levels in blood compared with those for [^{131}I]GV-620 and [^{131}I]GV-904. Uptake in lungs for the radioiodinated compounds followed a similar pattern as that for the ^{211}At-labeled analogues.

Because thyroid and stomach are known to sequester free astatide and iodide, activity levels in these tissues is a useful indicator of the relative in vivo stability of these radiohalogenated PSMA compounds. As shown in Fig. 5, stomach and thyroid radioactivity levels (%ID/organ) for the ^{211}At-labeled in general were higher ($P < 0.05$ except in thyroid for GV-620 at 4 h) than those for their radioiodinated counterparts as would be expected given their relative carbon-halogen bond strengths. Among these, [^{211}At]GV-620 administration resulted in the lowest %ID values at <0.2% at all time points, followed by [^{211}At]YC-550 (0.3–0.4%ID), [^{211}At]GV-904 (0.1–0.7%ID) and [^{211}At]HS-549 (0.8–0.9%ID). All novel ^{211}At-labeled analogues were more stable to deastatination than the first generation compound, [^{211}At]DCABzL (0.5–1.3%) [13]. Thyroid uptake of [^{131}I]GV-620 and [^{131}I]GV-904 was <0.1% ID, suggesting low susceptibility to in vivo deiodination while thyroid uptake of [^{131}I]HS-549 was higher ranging from 0.30 ± 0.13 %ID at 1 h to 0.08 ± 0.01%ID at 21 h. The %ID present in the stomach for the ^{211}At-labeled derivatives generally were considerably higher than those seen for the corresponding ^{131}I-labeled analogue (Fig. 5). Consistent with the results obtained for thyroid, [^{211}At]GV-620 had the lowest activity level in the stomach (0.9-.6%ID) while the highest stomach levels were seen with [^{211}At]HS-549 (3.2 −8.7%ID), which were similar to those observed for [^{211}At]DCABzL (3.8 – 8.2%) [13].

Tumor-to-normal tissue ratios calculated from the biodistribution studies are presented in Figs. 6 and 7 for the ^{211}At- and ^{131}I-labeled PSMA compounds, respectively, with the latter generally higher than the former. Tumor-to-blood and tumor-to-lung ratios were higher for [^{211}At]GV-620 and [^{211}At]GV-904 compared with that obtained for [^{211}At]HS-549. With respect to tumor-to-kidney ratios, [^{211}At]HS-549 had an advantage over other analogues. Except at 21 h for [^{211}At]GV-620, tumor-to-liver ratios for [^{211}At]YC-550 were higher than

that obtained for the other ^{211}At-labeled analogues. [^{211}At]HS-549 had higher the most favorable tumor-to-spleen ratios at 1 h and 2 h but [^{211}At]GV-620 had the highest at 21 h.

For the novel radioiodinated compounds, tumor-to-tissue ratios were generally higher than those observed previously for [^{131}I]DCIBzL [12, 13] and increased with time (Fig. 7). Tumor-to-kidney ratios for [^{131}I]HS-549 were 0.74 ± 0.15, 0.87 ± 0.30 and 6.26 ± 4.04 at 1 h, 2 h and 21 h, respectively. For [^{131}I]GV-620, they were <1 at early time points, reaching 2.64 ± 0.30 at 21 h. Similarly, for [^{131}I]GV-904 tumor-to-kidney ratios were <1 at 1 h and 2 h and attained a value of 9.9 ± 7.2 at 21 h. Tumor-to-blood ratios at later time points were substantially higher for [^{131}I]GV-620 and [^{131}I]GV-904 than for [^{131}I]DCIBzL. For example, values of 174 ± 102 (4 h) and 2,057 ± 1,110 (21 h) ([^{131}I]GV-620) and 150 ± 57 (2 h) and 1218 ± 675 (21 h) ([^{131}I]GV-904) were obtained compared with 98 ± 19 and 620 ± 243 for [^{131}I]DCIBzL. On the other hand, [^{131}I]HS-549 had low tumor-to-blood ratios of 13.3 ± 2.7, 26 ± 5.3 and 18 ± 19 at 1 h, 2 h and 21 h, respectively. Tumor-to-liver and tumor-to-lung ratios for [^{131}I]GV-620 and [^{131}I]GV-904 were higher than those for [^{131}I]HS-549; at early time points, [^{131}I]HS-549 had higher tumor-to-spleen ratios.

4. Discussion

In the present study, four novel PSMA ligands were successfully labeled with ^{211}At, one of the most attractive radionuclides for TAT. Although a variety of α-emitters have been evaluated in the context of PSMA-targeted radiotherapy [28], ^{211}At offers several important advantages including the emission of polonium K x-rays that can be imaged using conventional instrumentation and production of a single α-particle per decay [11]. The latter characteristic could provide important advantages compared with ^{225}Ac and ^{227}Th by avoiding problems associated with multiple α-particle emitting daughters that can be rapidly lost from the targeting vehicle resulting in normal tissue toxicity [29], reduction in relative biological effectiveness [30], and complicated radiation dosimetry [31]. However, a concern with ^{211}At is that its supply is constrained by the limited number of cyclotrons with the ~28–30 MeV α-particle beams needed for its efficient production [32]. The importance of addressing this problem has been recognized recently and efforts are under way in the European Union, Japan and the US to create consortia of accelerators with the goal of increasing ^{211}At supply. The second concern with ^{211}At-labeled radiopharmaceuticals is in vivo stability, a parameter that was evaluated in the current investigation. This was the main motivation for evaluating the corresponding ^{131}I-labeled compounds in paired-label experiments and comparing uptake in the thyroid and stomach, tissues known to sequester [^{131}I]iodide and [^{211}At]astatide [33].

As is often the case with ^{211}At-labeled radiopharmaceuticals, [^{211}At]DCABzL was selected based on prior experience with the radioiodinated version [34]. Biodistribution results for [^{211}At]DCABzL and [^{131}I]DCIBzL from Reference 13 have been included in the Figures to facilitate comparison with new compounds. On the positive side, [^{211}At]DCABzL was shown to bind specifically to PC3 PSMA+ PIP cells in vitro and exhibited >30% ID/g peak uptake in subcutaneous xenografts derived from this cell line [13]. Moreover, significant tumor growth delay was observed after a single injection of [^{211}At]DCABzL but not in isogenic PSMA-negative PC3 flu tumors. Finally, in a challenging micro-metastatic prostate

cancer mouse model characterized by disease spread to multiple sites in bone, liver and kidney, significant, dose-dependent prolongation in median survival was obtained with a single dose of [^{211}At]DCABzL. Taken together, these results show the promise of ^{211}At-labeled low molecular weight PSMA ligands for the treatment of mCRPC.

Unfortunately, there are two serious problems with the in vivo behavior of [^{211}At]DCABzL that make this compound unworthy of clinical translation – insufficient in vivo stability and high and prolonged retention of ^{211}At activity in the kidney. First, ^{211}At levels in the thyroid and stomach – tissues that sequester free astatide and iodide – were an order of magnitude higher than those for ^{131}I after co-administration of [^{211}At]DCABzL and [^{131}I]DCIBzL, suggesting that extensive deastatination had occurred. And second, as would be expected from the high and persistent renal uptake seen in the biodistribution studies, is that long-term toxicity studies in CD1 mice with [^{211}At]DCABzL demonstrated late radiation nephropathy after about 9 months, with loss of the proximal tubules, consistent with α-camera images showing intense uptake in this kidney substructure [13].

With the goal of addressing the limitations of [^{211}At]DCABzL while maintaining its benefits, the current study was undertaken to evaluate a small series of compounds that might provide higher in vivo stability and lower retention of ^{211}At activity in the kidneys. HS-549 has the same molecular weight as DCIBzL and a *K*i=0.01 nM, yet it contains a different pharmacophore for PSMA - (2-[3-(1,3-dicarboxypropyl)-ureido]-pentanedioic acid. Moreover, based on the work of Talanov et al. [35] with [^{211}At]SAPS and similar compounds, we hypothesized that positioning of the electron withdrawing amide group away from the aromatic ring (Figure 1) should offer an astatophenyl group that is more stable to dehalogenation compared to that in [^{211}At]DCABzL wherein the amide group is directly attached to the aromatic ring. Given that PSMA inhibitors are rapidly internalized, we also evaluated positively charged prosthetic groups bearing a pyridine or guanidine moiety that have been shown to enhance cellular retention of ^{211}At when used for labeling internalizing mAbs [14, 15]. These studies also showed a low degree of deastatination for mAbs labeled using these prosthetic agents and similar biodistribution patterns for the ^{211}At- and ^{131}I-labeled mAb conjugates in paired-label studies. Finally, experiments evaluating the biodistribution of likely low-molecular-weight catabolites generated from mAbs labeled with radioiodinated versions demonstrated low retention of activity in normal tissues, particularly in kidneys [36]. To evaluate the potential utility of pyridine and guanidine moieties for ^{211}At-labeled PSMA inhibitors, [^{211}At]YC-550 and [^{211}At]GV-620, respectively (Fig. 1), were synthesized. [^{211}At]GV-904, that includes a long linker in case the guanidino prosthetic group in [^{211}At]GV-620 was too bulky to fit in the non-pharmacophore binding pocket of PSMA, also was synthesized.

In this study, we utilized the most commonly used method for the synthesis of the ^{211}At-labeled compounds electrophilic astatodestannylation [37, 38]. Radiochemical yields are generally are greater than 50% for this reaction, which was the case with [^{211}At]HS-549, [^{211}At]GV-620 and [^{211}At]GV-904. However, the average RCY for [^{211}At]YC-550 was only 34%. We note that compared with benzene, the reaction rate for aromatic electrophilic substitution on pyridine is much slower due to electronegativity of nitrogen. Consistent with this, lower radiochemical yields for radioiodinated YC-550 compared with DCIBzL

analogue has been reported [12]. In addition, the bulkier tri-n-butyl tin group (vs trimethyl) can also contribute to a lower labeling yield, particularly with the more bulky astatine atom. [^{211}At]YC-550 was synthesized only three times; while a RCY of 62% was obtained once, RCY were 20% and 15% for the other 2 runs. Electrophilic labeling efficiency with ^{211}At is dependent on the initial quality of the ^{211}At, which can vary depending the radiation dose received before the labeling reaction is carried out [16]. Finally, exploiting recently developed pathways for ^{211}At labeling via nucleophilic substitution of boronate [39] or iodonium salt precursors [40] might provide a higher and more consistent RCY.

Relative stability towards in vivo dehalogenation was assessed by comparing uptake of radioactivity in thyroid and stomach, the tissues most avidly accumulating astatide and iodide. An additional signature of astatide but not iodide release is unexpected uptake of ^{211}At in spleen and lungs [33]. Consistent with the lower C-X bond strength for astatine, thyroid and stomach uptake for each ^{211}At-labeled PSMA inhibitor was significantly higher than observed for its co-administered ^{131}I-labeled analogue (Tables 1–4). The higher rate of dehalogenation for the ^{211}At-labeled analogues compared with their ^{131}I-labeled counterparts likely also contributed to their lower uptake in tumor as well as higher uptake in spleen and lungs. Both benzene ring-bearing agents - [^{211}At]DCABzL and [^{211}At]HS-549 – resulted in the highest activity levels in thyroid and stomach while pyridine-containing [^{211}At]YC-550 had levels about half of those.

The guanidino prosthetic agent bearing [^{211}At]GV-620 was by far the most stable towards in vivo deastatination with <0.2 %ID in the thyroid at all time points, a value only 2–4 times higher than that for co-administered [^{131}I]GV-620. In comparison, the uptake of [^{211}At]astatide in the thyroid has been reported to be about 0.6–1.7 %ID over a similar time period [41]. The results obtained with [^{211}At]GV-620 are a marked improvement over those obtained with first-generation compound [^{211}At]DCABzL and consistent with those reported previously when a structurally similar [^{211}At]SAGMB agent was used to label a 13-kDa single domain antibody fragment [42] as well as for *m*-[^{211}At]astatobenzylguanidine [41, 43].

Motivated by the late stage renal toxicity observed with [^{211}At]DCABzL, our second objective was to develop a ^{211}At-labeled PSMA inhibitor with less sequestration in the kidneys while maintaining good uptake in PSMA+ tumors. Although we suspect that all of the compounds will be more concentrated in renal tubules than other regions of the kidney [13], the activity in the whole kidney was used for the purposes of comparing these compounds. Kidney activity of ^{211}At was lowest for [^{211}At]HS-549; however, the extensive dehalogenation of this compound presumably contributes to this behavior and makes this compound unattractive for clinical development. All of the other ^{211}At-labeled analogues (as well as their corresponding ^{131}I-labeled derivatives) exhibited somewhat higher kidney activity than [^{211}At]DCABzL but notably, unlike the first generation compound, cleared to about 5% of 1 h levels at 18–21 h. This suggests that ^{211}At labeling of PSMA inhibitors via pyridine- or guanidine- bearing acylation agents may be a useful strategy for mitigating late-stage renal toxicity.

There was some differentiation among the three positive-charge-prosthetic-agent bearing ^{211}At-labeled PSMA inhibitors with good in vivo stability and rapid kidney clearance on the basis of tumor-to-normal tissue ratios. Tumor-to-tissue ratios in blood, lungs and spleen for both [^{211}At]GV-620 and [^{211}At]GV-904 were higher than those for the pyridine-containing compound at all time points. Differentiation between [^{211}At]GV-620 and the additional candidates was most apparent at 18–21 h. With the exception of kidney, tumor-to-normal tissue ratios at 18–21 h for [^{211}At]GV-620 were higher than those for the other guanidine containing compound, [^{211}At]GV-904, particularly in the small intestine, consistent with the higher lipophilicity of the later. These trends are mirrored by the results observed with the ^{131}I-labeled analogues supporting the important role that the radiohalogenated prosthetic agent plays in determining the in vivo behavior of PSMA inhibitor radioconjugates.

5. Conclusion

In summary, we have synthesized four novel ^{211}At-labeled PSMA inhibitors as well as their ^{131}I-labeled analogues. The new ^{211}At-labeled compounds offered significant advantages in terms of in vivo stability, kidney retention or both, with the nature of the ^{211}At-labeled prosthetic group having a profound effect on in vivo behavior. Based on this work, the guanidine containing [^{211}At]GV-620 emerged as the lead and will be evaluated further as a potential agent for TAT of mCRPC.

Supplementary Material

Refer to Web version on PubMed Central for supplementary material.

Acknowledgements

The authors acknowledge the support of the National Cancer Institute for providing research support under Grant CA184228. We also wish to thank Shawn Murphy and Michael Daily for their assistance in performing the ^{211}At production cyclotron irradiations and target distillations. We thank Dr. Warren Heston for providing the PSMA+ PC3 PIP and PSMA- PC3 flu cells.

References

[1]. Vaishampayan U. Therapeutic options and multifaceted treatment paradigms in metastatic castrate-resistant prostate cancer. Curr Opin Oncol 2014;26:265–73. [PubMed: 24626129]

[2]. Giammarile F, Mognetti T, and Resche I. Bone pain palliation with strontium-89 in cancer patients with bone metastases. Q J Nucl Med 2001;45:78–83. [PubMed: 11456379]

[3]. Serafini AN. Systemic metabolic radiotherapy with samarium-153 EDTMP for the treatment of painful bone metastasis. Q J Nucl Med 2001;45:91–9. [PubMed: 11456381]

[4]. Rowe SP, Drzezga A, Neumaier B, Dietlein M, Gorin MA, Zalutsky MR, et al. Prostate-Specific Membrane Antigen-Targeted Radiohalogenated PET and Therapeutic Agents for Prostate Cancer. J Nucl Med 2016;57:90–6S.

[5]. Kratochwil C, Haberkorn U, and Giesel FL. Radionuclide Therapy of Metastatic Prostate Cancer. Semin Nucl Med 2019;49:313–25. [PubMed: 31227054]

[6]. Hofman MS, Violet J, Hicks RJ, Ferdinandus J, Thang SP, Akhurst T, et al. [177Lu]-PSMA-617 radionuclide treatment in patients with metastatic castration-resistant prostate cancer (LuPSMA trial): a single-centre, single-arm, phase 2 study. Lancet Oncol 2018;19:825–33. [PubMed: 29752180]

[7]. Zang J, Fan X, Wang H, Liu Q, Wang J, Li H, et al. First-in-human study of ^{177}Lu-EB-PSMA-617 in patients with metastatic castration-resistant prostate cancer. Eur J Nucl Med Mol Imaging 2019;46:148–58. [PubMed: 30090965]

[8]. Parker C, Nilsson S, Heinrich D, Helle SI, O'Sullivan JM, Fossa SD, et al. Alpha emitter radium-223 and survival in metastatic prostate cancer. N Engl J Med 2013;369:213–23. [PubMed: 23863050]

[9]. Poty S, Francesconi LC, McDevitt MR, Morris MJ, and Lewis JS. alpha-Emitters for Radiotherapy: From Basic Radiochemistry to Clinical Studies-Part 1. J Nucl Med 2018;59:878–84. [PubMed: 29545378]

[10]. Kratochwil C, Bruchertseifer F, Giesel FL, Weis M, Verburg FA, Mottaghy F, et al. ^{225}Ac-PSMA-617 for PSMA-Targeted alpha-Radiation Therapy of Metastatic Castration-Resistant Prostate Cancer. J Nucl Med 2016;57:1941–4. [PubMed: 27390158]

[11]. Vaidyanathan G and Zalutsky MR. Applications of 211At and 223Ra in targeted alpha-particle radiotherapy. Curr Radiopharm 2011;4:283–94. [PubMed: 22202151]

[12]. Chen Y, Foss CA, Byun Y, Nimmagadda S, Pullambhatla M, Fox JJ, et al. Radiohalogenated prostate-specific membrane antigen (PSMA)-based ureas as imaging agents for prostate cancer. J Med Chem 2008;51:7933–43. [PubMed: 19053825]

[13]. Kiess AP, Minn I, Vaidyanathan G, Hobbs RF, Josefsson A, Shen C, et al. (2S)-2-(3-(1-Carboxy-5-(4–211At-Astatobenzamido)Pentyl)Ureido)-Pentanedioic Acid for PSMA-Targeted alpha-Particle Radiopharmaceutical Therapy. J Nucl Med 2016;57:1569–75. [PubMed: 27230930]

[14]. Reist CJ, Foulon CF, Alston K, Bigner DD, and Zalutsky MR. Astatine-211 labeling of internalizing anti-EGFRvIII monoclonal antibody using N-succinimidyl 5-[211At]astato-3-pyridinecarboxylate. Nucl Med Biol 1999;26:405–11. [PubMed: 10382844]

[15]. Vaidyanathan G, Affleck DJ, Bigner DD, and Zalutsky MR. N-succinimidyl 3-[211At]astato-4-guanidinomethylbenzoate: an acylation agent for labeling internalizing antibodies with alpha-particle emitting 211At. Nucl Med Biol 2003;30:351–9. [PubMed: 12767391]

[16]. Pozzi OR and Zalutsky MR. Radiopharmaceutical chemistry of targeted radiotherapeutics, Part 3: alpha-particle-induced radiolytic effects on the chemical behavior of ^{211}At. J Nucl Med 2007;48:1190–6. [PubMed: 17574991]

[17]. Zalutsky MR, Zhao XG, Alston KL, and Bigner D. High-level production of alpha-particle-emitting ^{211}At and preparation of ^{211}At-labeled antibodies for clinical use. J Nucl Med 2001;42:1508–15. [PubMed: 11585865]

[18]. Vaidyanathan G and Zalutsky MR. Synthesis of N-succinimidyl 4-guanidinomethyl-3-[*I]iodobenzoate: a radio-iodination agent for labeling internalizing proteins and peptides. Nat Protoc 2007;2:282–6. [PubMed: 17406587]

[19]. Kularatne SA, Zhou Z, Yang J, Post CB, and Low PS. Design, synthesis, and preclinical evaluation of prostate-specific membrane antigen targeted ^{99m}Tc-radioimaging agents. Mol Pharm 2009;6:790–800. [PubMed: 19361232]

[20]. Kurth M, Pelegrin A, Rose K, Offord RE, Pochon S, Mach JP, et al. Site-specific conjugation of a radioiodinated phenethylamine derivative to a monoclonal antibody results in increased radioactivity localization in tumor. J Med Chem 1993;36:1255–61. [PubMed: 8487262]

[21]. Banerjee SR, Kumar V, Lisok A, Chen J, Minn I, Brummet M, et al. ^{177}Lu-labeled low-molecular-weight agents for PSMA-targeted radiopharmaceutical therapy. Eur J Nucl Med Mol Imaging 2019;46:2545–57. [PubMed: 31399803]

[22]. Maresca KP, Hillier SM, Femia FJ, Keith D, Barone C, Joyal JL, et al. A series of halogenated heterodimeric inhibitors of prostate specific membrane antigen (PSMA) as radiolabeled probes for targeting prostate cancer. J Med Chem 2009;52:347–57. [PubMed: 19111054]

[23]. Olszewski RT, Bukhari N, Zhou J, Kozikowski AP, Wroblewski JT, Shamimi-Noori S, et al. NAAG peptidase inhibition reduces locomotor activity and some stereotypes in the PCP model of schizophrenia via group II mGluR. J Neurochem 2004;89:876–85. [PubMed: 15140187]

[24]. Banerjee SR, Pullambhatla M, Shallal H, Lisok A, Mease RC, and Pomper MG. A modular strategy to prepare multivalent inhibitors of prostate-specific membrane antigen (PSMA). Oncotarget 2011;2:1244–53. [PubMed: 22207391]

[25]. Cheng Y and Prusoff WH. Relationship between the inhibition constant (K1) and the concentration of inhibitor which causes 50 per cent inhibition (I50) of an enzymatic reaction. Biochem Pharmacol 1973;22:3099–108. [PubMed: 4202581]

[26]. Benesova M, Schafer M, Bauder-Wust U, Afshar-Oromieh A, Kratochwil C, Mier W, et al. Preclinical Evaluation of a Tailor-Made DOTA-Conjugated PSMA Inhibitor with Optimized Linker Moiety for Imaging and Endoradiotherapy of Prostate Cancer. J Nucl Med 2015;56:914–20. [PubMed: 25883127]

[27]. Meyer GJ, Walte A, Sriyapureddy SR, Grote M, Krull D, Korkmaz Z, et al. Synthesis and analysis of 2-[^{211}At]-L-phenylalanine and 4-[^{211}At]-L-phenylalanine and their uptake in human glioma cell cultures in-vitro. Appl Radiat Isot 2010;68:1060–5. [PubMed: 20137958]

[28]. Czerwinska M, Bilewicz A, Kruszewski M, Wegierek-Ciuk A, and Lankoff A. Targeted Radionuclide Therapy of Prostate Cancer-From Basic Research to Clinical Perspectives. Molecules 2020;25.

[29]. de Kruijff RM, Wolterbeek HT, and Denkova AG. A Critical Review of Alpha Radionuclide Therapy-How to Deal with Recoiling Daughters? Pharmaceuticals (Basel) 2015;8:321–36. [PubMed: 26066613]

[30]. Ackerman NL, de la Fuente Rosales L, Falzone N, Vallis KA, and Bernal MA. Targeted alpha therapy with 212Pb or 225Ac: Change in RBE from daughter migration. Phys Med 2018;51:91–8. [PubMed: 29807854]

[31]. Sgouros G, Bodei L, McDevitt MR, and Nedrow JR. Radiopharmaceutical therapy in cancer: clinical advances and challenges. Nat Rev Drug Discov 2020;19:589–608. [PubMed: 32728208]

[32]. Zalutsky MR and Pruszynski M. Astatine-211: production and availability. Curr Radiopharm 2011;4:177–85. [PubMed: 22201707]

[33]. Larsen RH, Slade S, and Zalutsky MR. Blocking [211At]astatide accumulation in normal tissues: preliminary evaluation of seven potential compounds. Nucl Med Biol 1998;25:351–357. [PubMed: 9639296]

[34]. Kiess AP, Minn I, Chen Y, Hobbs R, Sgouros G, Mease RC, et al. Auger Radiopharmaceutical Therapy Targeting Prostate-Specific Membrane Antigen. J Nucl Med 2015;56:1401–7. [PubMed: 26182968]

[35]. Talanov VS, Yordanov AT, Garmestani K, Milenic DE, Arora HC, Plascjak PS, et al. Preparation and in vivo evaluation of novel linkers for 211At labeling of proteins. Nucl Med Biol 2004;31:1061–71. [PubMed: 15607488]

[36]. Vaidyanathan G, Affleck DJ, Bigner DD, and Zalutsky MR. Improved xenograft targeting of tumor-specific anti-epidermal growth factor receptor variant III antibody labeled using N-succinimidyl 4-guanidinomethyl-3-iodobenzoate. Nucl Med Biol 2002;29:1–11. [PubMed: 11786270]

[37]. Aneheim E, Foreman MRStJ, Jensen H, and Lindegren S. N-[2-(maleimido)ethyl]-3-(trimethylstannyl)benzamide, a molecule for radiohalogenation of proteins and peptides. Appl Rad Isot 2015;96:1–5.

[38]. Ogawa K, Takeda T, Mishiro K, Toyoshima A, Shiba K, Yoshimura T, et al. Radiotheranostics coupled between an At-211-labeled RGD peptide and the corresponding radioiodine-labeled RGD peptide. ACS Omega 2019;4:4584–4591.

[39]. Reilly SW, Makvandi M, Xu K, and Mach RH. Rapid Cu-catalyzed [211At]astatination and [125I]iodination of boronic esters at room temperature. Org Lett 2018;20:1752–1755. [PubMed: 29561158]

[40]. Navarro L, Berdal M, Chérel M, Pecorari F, Gestin J-F, and Guérard F. Prosthetic groups for radioiodination and astatination of peptides and proteins: a comparative study of five potential bioorthogonal labeling strategies. Bioorg Med Chem 2019;27:167–174. [PubMed: 30529152]

[41]. Ukon N, Zhao S, Washiyama K, et al. Human dosimetry of free 211At and meta-[211At]astatobenzylguanidine (211At-MABG) estimated using preclinical biodistribution from normal mice. EJNMMI Physics 2020;7:58. [PubMed: 32960387]

[42]. Choi J, Vaidyanathan G, Koumarianou E, Kang CM, and Zalutsky MR. Astatine-211 labeled anti-HER2 5F7 single domain antibody fragment conjugates: radiolabeling and preliminary evaluation. Nucl Med Biol 2018;56:10–20. [PubMed: 29031230]

[43]. Vaidyanathan G and Zalutsky MR. 1-(m-[211At]astatobenzyl)guanidine: synthesis via astato demetalation and preliminary in vitro and in vivo evaluation. Bioconjug Chem 1992;3:499–503. [PubMed: 1463779]

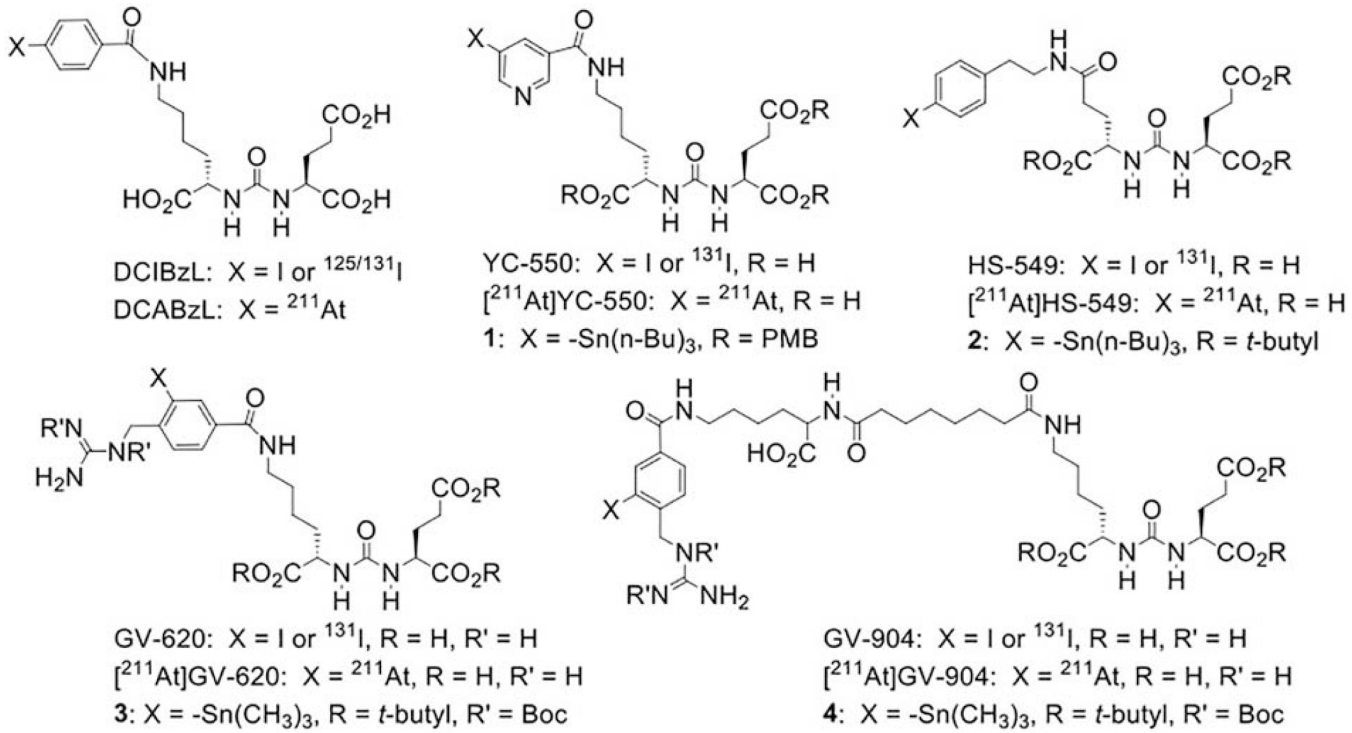

Figure 1.

Structures of standards, and ^{131}I-labeled and ^{211}At-labeled analogues of PSMA inhibitors used in this work as well as their tin precursors.

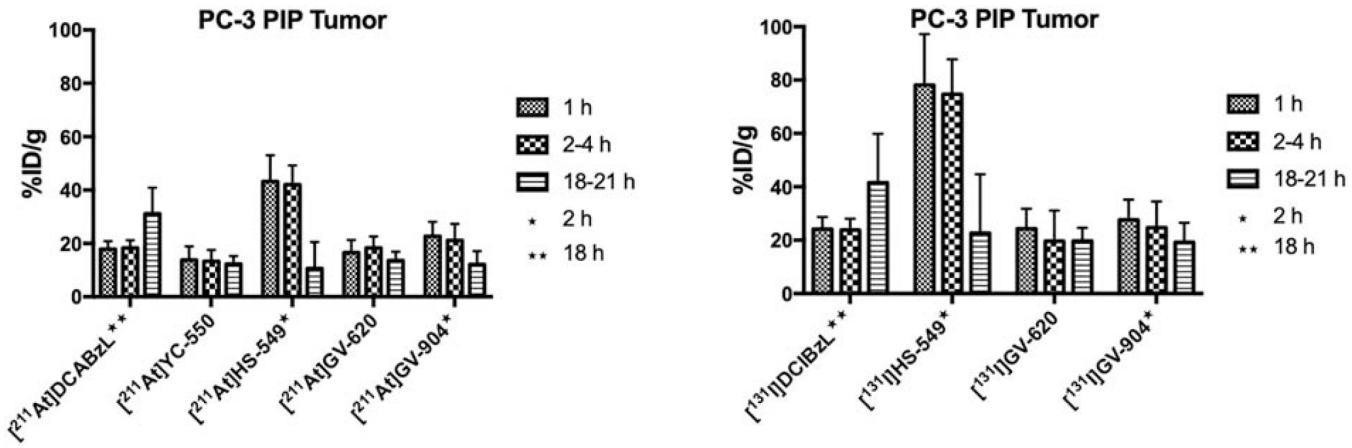

Figure 2.

Uptake of ^{211}At and ^{131}I activity after injection of ^{211}At- and ^{131}I-labeled PSMA inhibitors in subcutaneous PSMA+ PC3 PIP subcutaneous xenografts.

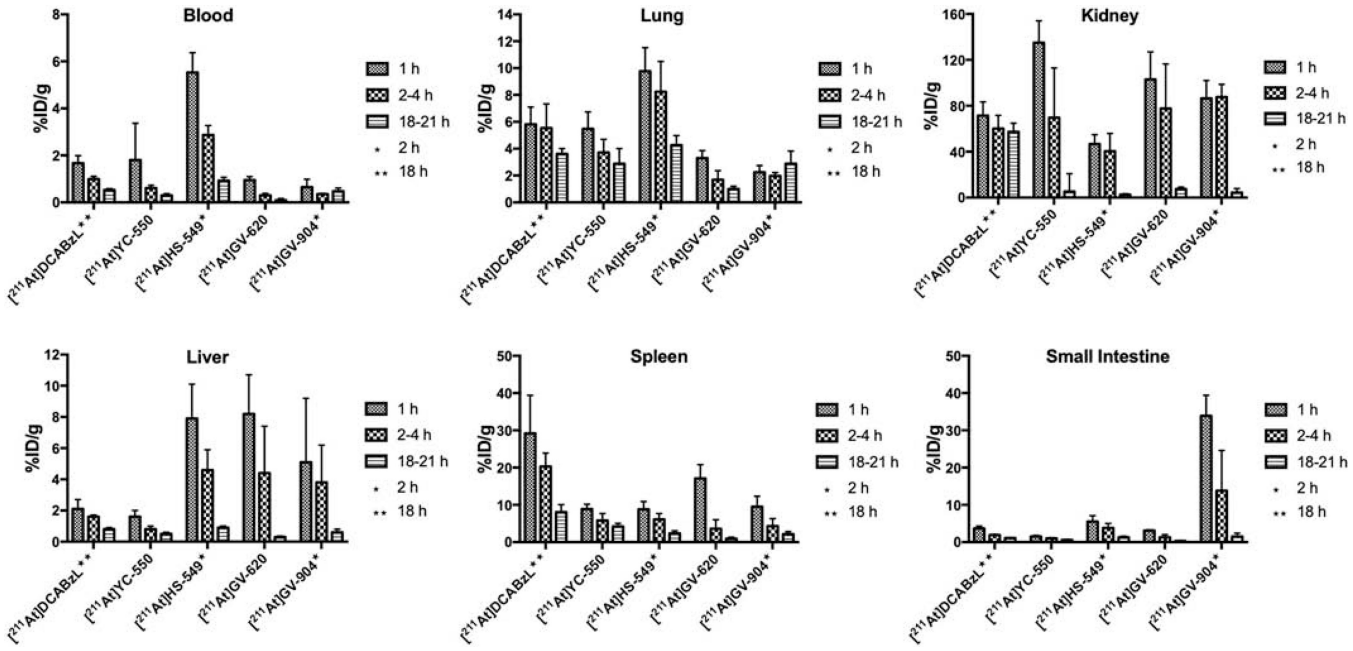

Figure 3.

Normal tissue distribution of ^{211}At activity, expressed as % injected dose per gram tissue, in mice injected with ^{211}At-labeled PSMA inhibitors.

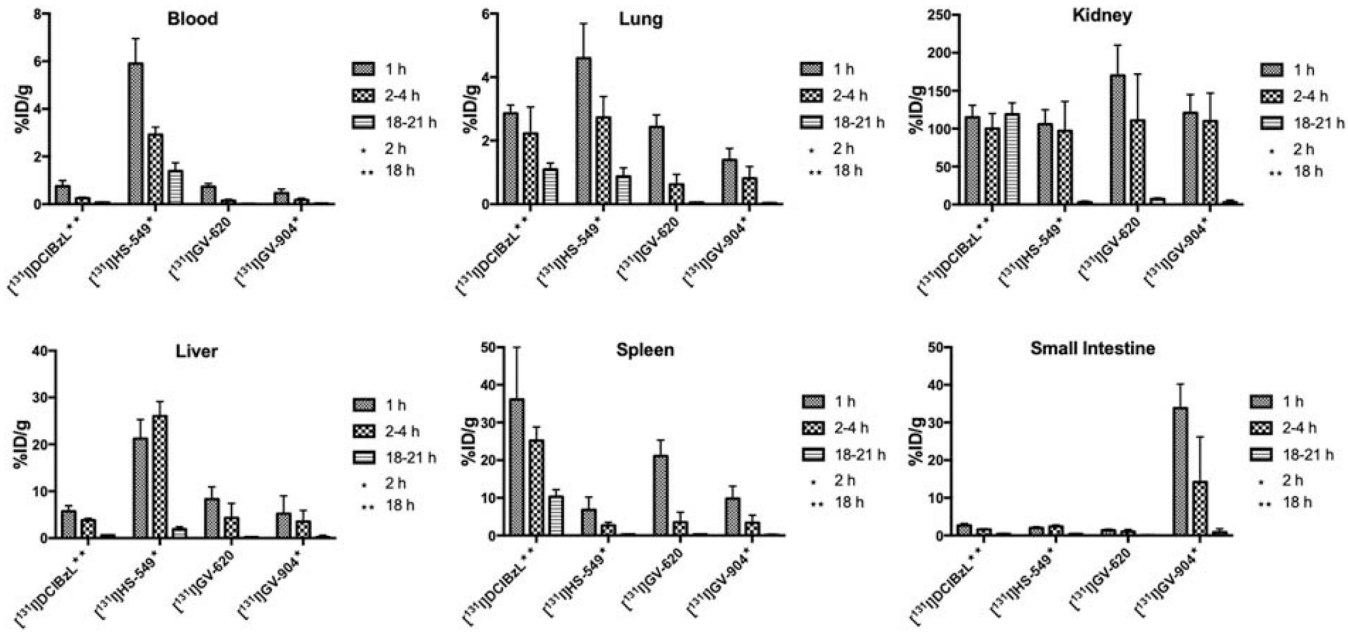

Figure 4.

Normal tissue distribution of ^{131}I activity, expressed as % injected dose per gram tissue, in mice injected with ^{131}I-labeled PSMA inhibitors.

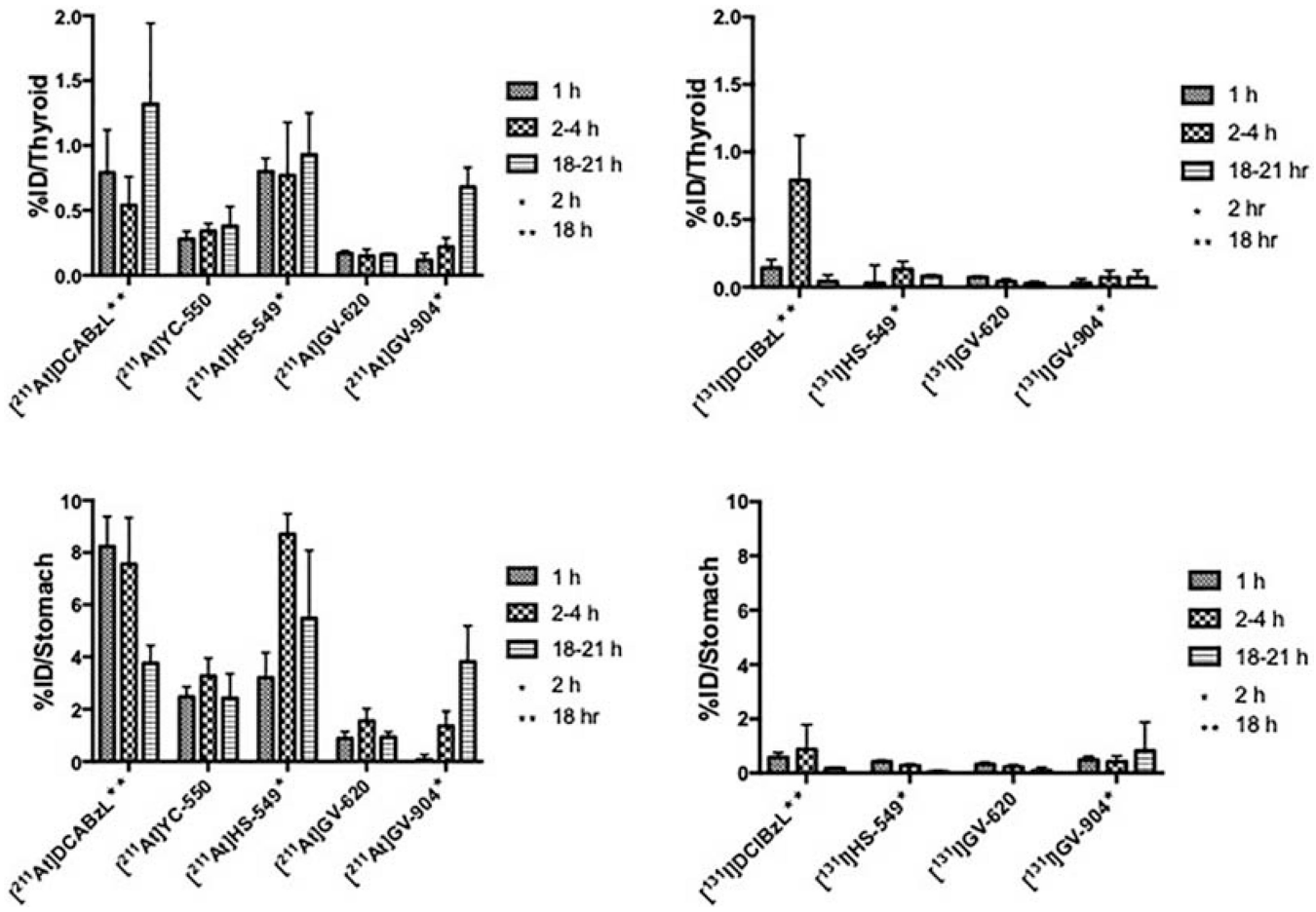

Figure 5.

Percentage of the injected dose of ^{211}At and ^{131}I activity present in the thyroid and the stomach after injection of ^{211}At- and ^{131}I-labeled PSMA inhibitors.

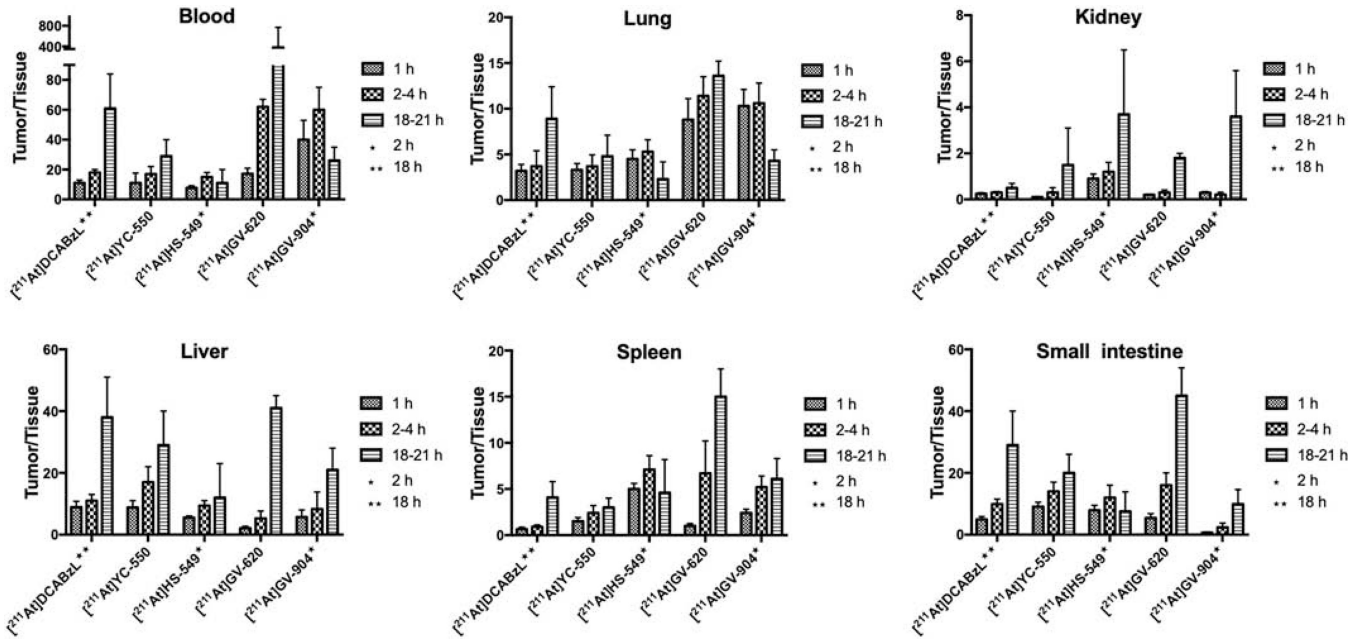

Figure 6.

PSMA+ PC3 PIP tumor-to-normal tissue ratios of ^{211}At activity after injection of ^{211}At-labeled PSMA inhibitors.

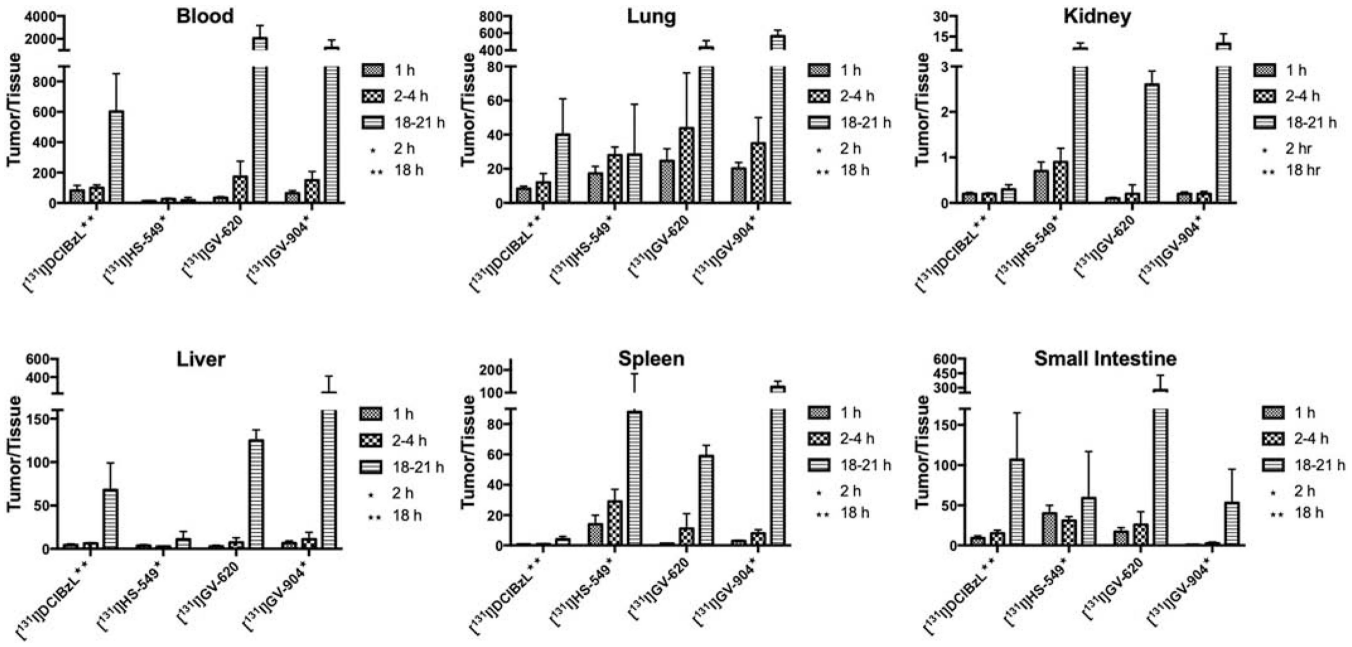

Figure 7.

PSMA+ PC3 PIP tumor-to-normal tissue ratios of ^{131}I activity after injection of ^{131}I-labeled PSMA inhibitors.

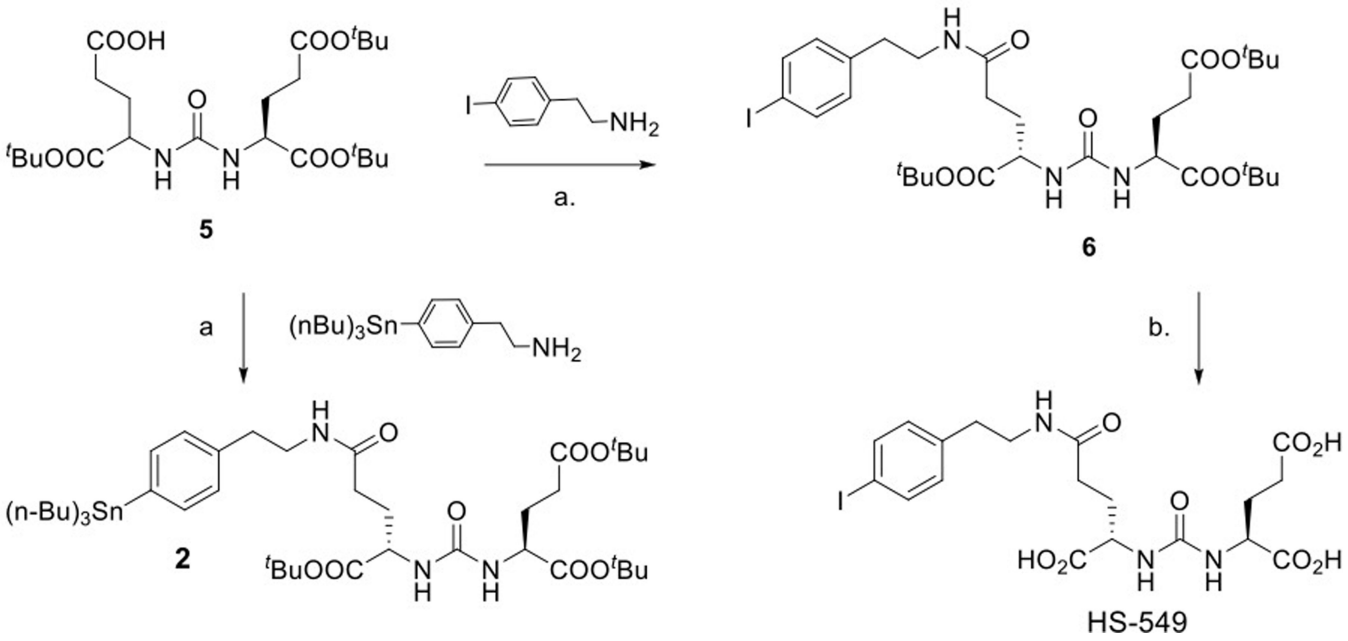

Scheme 1.

Synthesis of HS-549 and its tin precursor **2**. a) TSTU, DIPEA, DMF; b. TFA/CH_2CH_2.

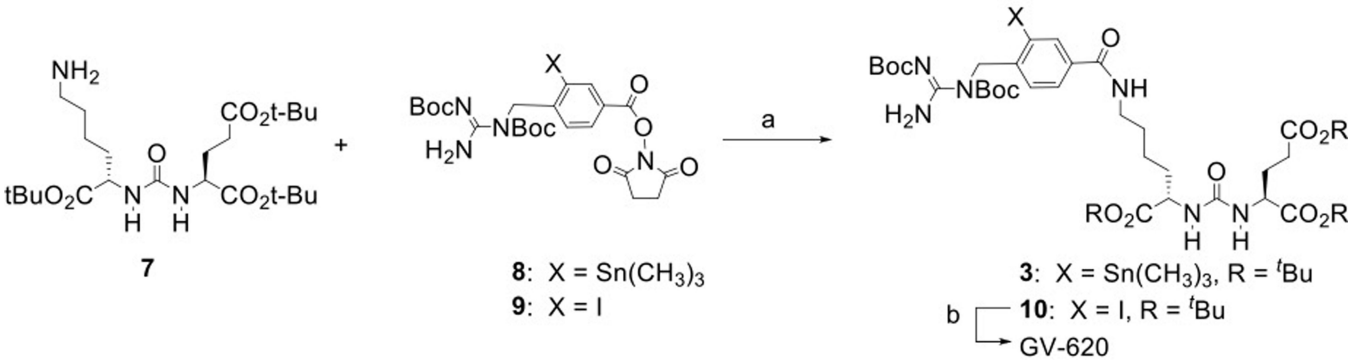

Scheme 2.

Synthesis of GV-620 and its tin precursor. a) triethylamine, dichloromethane; b) trifluoroacetic acid.

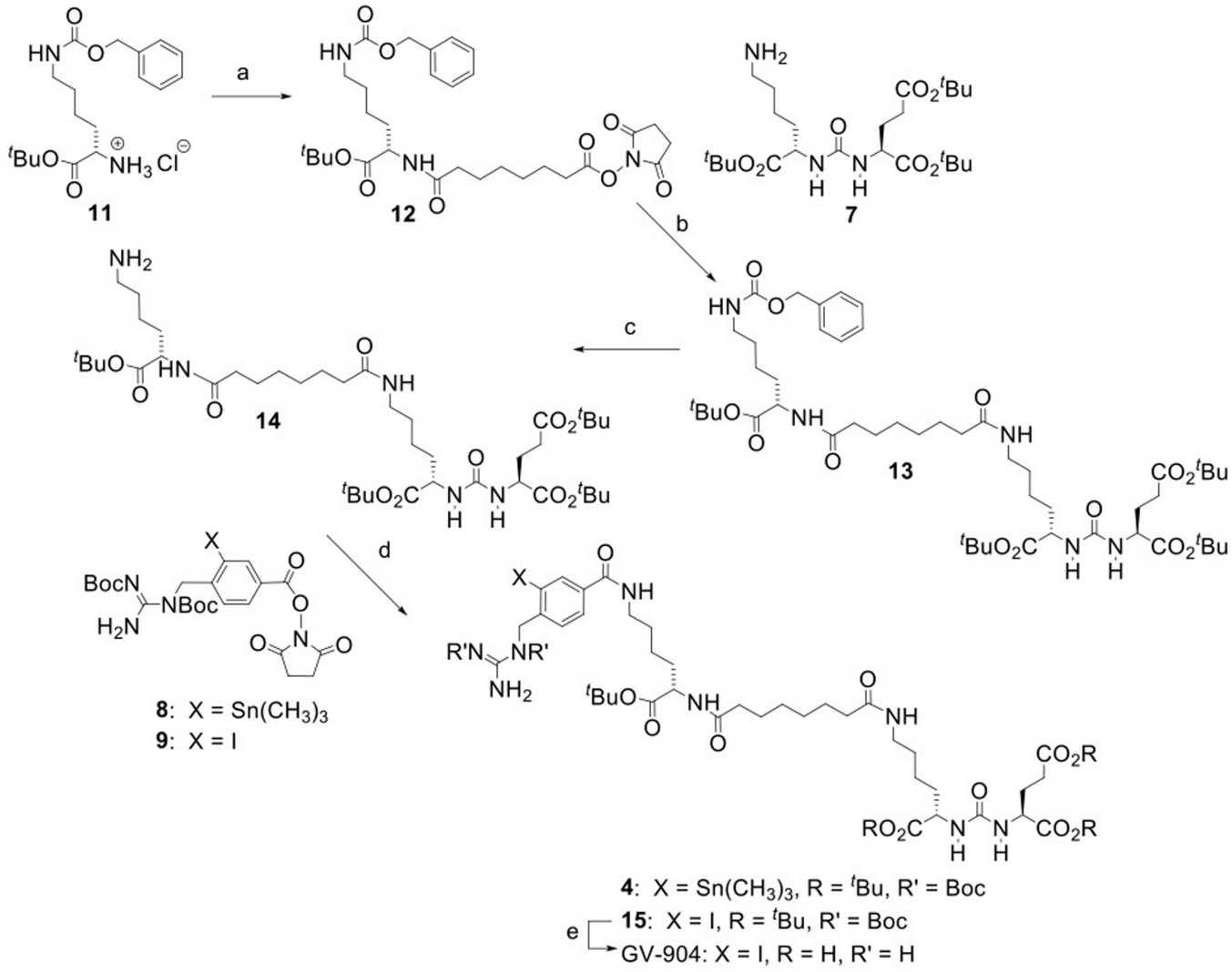

Scheme 3.

Synthesis of GV-904 and its tin precursor **4**. a) disuccinimidyl suberate, triethylamine, acetonitrile; b) triethylamine, acetonitrile; c) ammonium formate, Pd/C, ethanol, H_2; d) triethylamine, dichloromethane; e) trifluoroacetic acid.

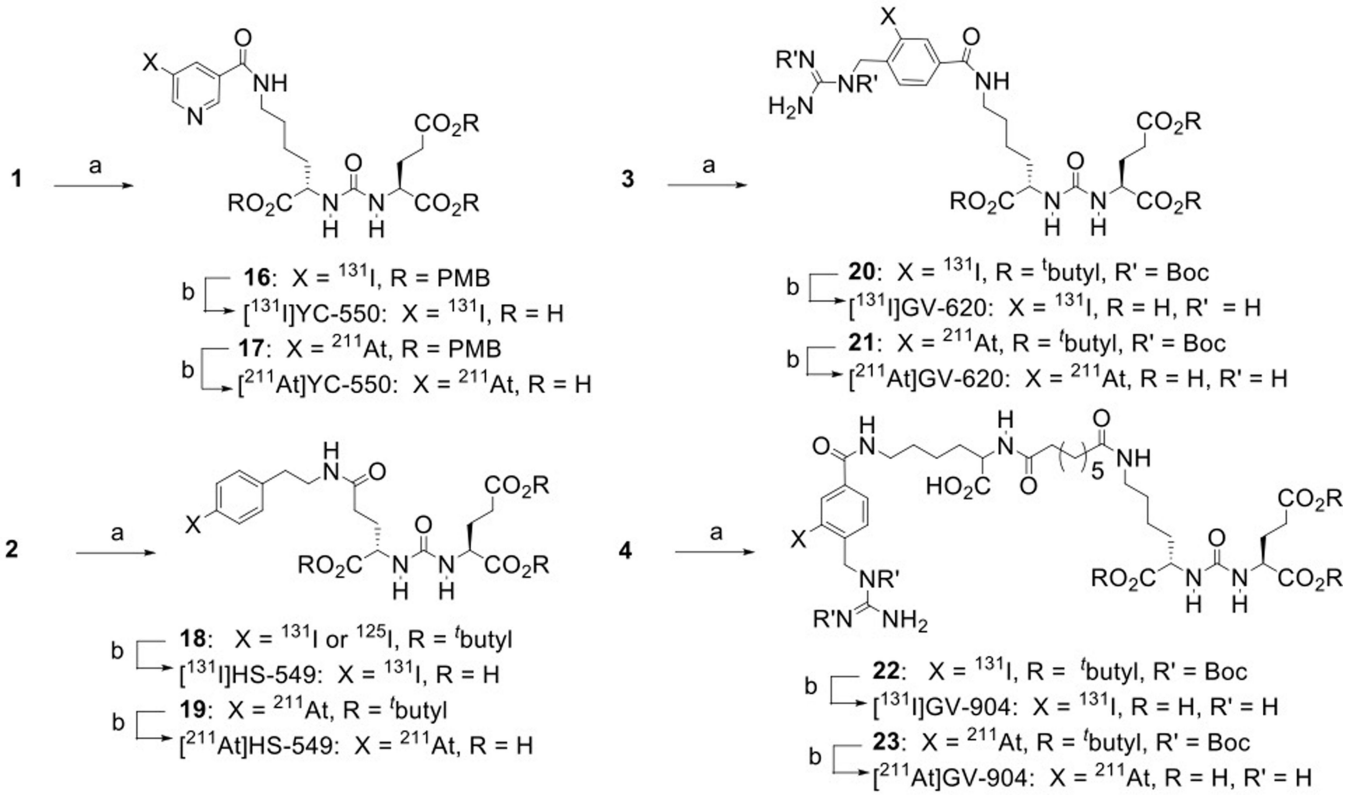

Scheme 4.

Synthesis of radiohalogenated PSMA inhibitors. a) ^{211}At or ^{131}I, *N*-chlorosuccinimide, acetic acid, 10 min, room temperature; b) anisole/trifluoroacetic acid or 100% trifluoroacetic acid.

Table 1.

Biodistribution of [^{211}At]YC-550 in athymic mice bearing PC-3 PIP and PC-3 flu xenografts

Tissue	Percent injected dose per gram[a]			
	1 h	2 h	4 h	21 h
Liver	1.56 ± 0.35	1.20 ± 0.27	0.79 ± 0.17	0.46 ± 0.12
Spleen	8.87 ± 1.33	8.00 ± 2.08	5.83 ± 1.91	4.23 ± 0.84
Lungs	5.48 ± 1.26	4.62 ± 1.06	3.72 ± 0.98	2.89 ± 1.12
Heart	1.67 ± 0.27	1.25 ± 0.28	1.27 ± 0.30	0.91 ± 0.33
Kidneys	135.3 ± 18.9	124.2 ± 23.6	69.6 ± 43.4	5.4 ± 15.5
Stomach	5.37 ± 0.61	6.24 ± 2.99	8.30 ± 2.26	4.30 ± 1.24
Sm. Int.	1.48 ± 0.29	1.21 ± 0.42	0.95 ± 0.21	0.63 ± 0.13
Lg. Int.	0.41 ± 0.10	0.70 ± 0.25	0.73 ± 0.20	0.63 ± 0.10
Thyroid	1.64 ± 0.25	1.85 ± 0.36	2.02 ± 0.27	2.22 ± 1.04
Muscle	0.53 ± 0.15	0.43 ± 0.11	0.40 ± 0.21	0.26 ± 0.10
Blood	1.80 ± 1.57	0.64 ± 0.11	0.61 ± 0.12	0.30 ± 0.07
Bone	1.15 ± 0.28	1.09 ± 0.23	0.86 ± 0.29	0.40 ± 0.25
Brain	0.20 ± 0.05	0.19 ± 0.04	0.16 ± 0.03	0.09 ± 0.02
PC-3 PIP	13.77 ± 5.06	15.16 ± 4.68	13.29 ± 4.19	12.34 ± 3.01
PC-3 flu	1.38 ± 0.22	1.19 ± 0.24	1.12 ± 0.20	0.57 ± 0.19

[a]Data obtained from a paired label biodistribution of [^{211}At]YC-550 and [^{131}I]DCIBzL; Mean ± SD (n = 5).

Table 2.

Paired label biodistribution of [^{211}At]HS-549 and [^{131}I]HS-549 in SCID mice bearing PC-3 PIP and PC-3 flu xenografts

Tissue	Percent injected dose per gram[a]					
	[^{211}At]HS-549			[^{131}I]HS-549		
	1 h	2 h	21 h	1 h	2 h	21 h
Liver	7.94 ± 2.15	4.65 ±1.28	0.89 ± 0.13	21.2± 4.14	26.0 ± 3.09	1.86 ± 0.51
Spleen	8.79 ± 2.09	6.13 ± 1.59	2.31 ± 0.67	6.76 ± 3.42	2.71 ± 0.85	0.29 ± 0.12
Lungs	9.77 ± 1.75	8.24 ± 2.25	4.26 ± 0.72	4.60 ± 1.09	2.73 ± 0.66	0.87 ± 0.27
Heart	4.34 ± 0.96	3.36 ± 0.59	1.64 ± 0.54	2.30 ± 0.63	1.14 ± 0.18	0.41 ± 0.09
Kidneys	46.7 ± 8.2	40.4 ± 15.5	2.60 ± 0.77	106 ± 18.9	96.6 ± 39.1	3.13 ± 1.65
Stomach	7.07 ± 2.24	14.3 ± 3.2	12.6 ± 6.20	0.92 ± 0.20	0.47 ± 0.17	0.14 ± 0.04
Sm. Int.	5.52 ± 1.57	3.81 ± 1.24	1.28 ± 0.30	1.98 ± 0.30	2.42 ± 0.40	0.37 ± 0.06
Lg. Int.	1.16 ± 0.20	4.59 ± 0.81	0.93 ± 0.41	0.52 ± 0.12	1.32 ± 0.25	0.63 ± 0.39
Thyroid	3.24 ± 0.56	4.11 ± 2.00	3.78 ± 0.63	1.17 ± 0.43	0.69 ± 0.29	0.36 ± 0.05
Muscle	1.11 ± 0.29	0.76 ± 0.18	0.29 ± 0.09	0.86 ± 0.26	0.46 ± 0.12	0.16 ± 0.04
Blood	5.53 ± 0.84	2.87 ± 0.40	0.92 ± 0.15	5.90 ± 1.05	2.92 ± 0.32	1.39 ± 0.35
Bone	1.49 ± 0.40	1.27 ± 0.30	0.60 ± 0.17	0.94 ± 0.36	0.65 ± 0.25	0.20 ± 0.05
Brain	0.46 ± 0.09	0.39 ± 0.06	0.17 ± 0.03	0.26 ± 0.08	0.18 ± 0.02	0.08 ± 0.02
PC-3 PIP	43.2 ± 9.8	42.0 ± 7.16	10.6 ± 9.91	78.1 ± 19.1	74.7 ± 13.1	22.6 ± 22.1
PC-3 flu	3.48 ± 0.53	2.82 ±0.60	1.15 ± 0.32	2.21 ± 0.53	1.51 ± 0.30	0.44 ± 0.18

[a]Mean ± SD (n = 5).

Table 3.

Paired label biodistribution of [^{211}At]GV-620 and [^{131}I]GV-620 in SCID mice bearing PC-3 PIP and PC-3 flu xenografts

Tissue	Percent injected dose per gram[a]									
	[^{211}At]GV-620					[^{131}I]GV-620				
	1 h	2 h	4 h	14 h	21 h	1 h	2 h	4 h	14 h	21 h
Liver	8.25±2.47	5.62±1.17	4.37±2.96	0.60±0.28	0.33±0.06	8.27±2.65	5.73±1.20	4.31±3.08	0.38±0.26	0.16±0.03
Spleen	17.1±3.71	6.81±3.20	3.63±2.40	1.27±0.42	0.93±0.37	21.1±4.2	7.31±3.73	3.50±2.69	0.50±0.20	0.33±0.07
Lungs	3.29±0.56	1.99±0.23	1.69±0.67	1.02±0.27	1.02±0.21	2.43±0.38	1.06±0.15	0.62±0.32	0.09±0.03	0.05±0.01
Heart	1.29±0.37	0.89±0.18	0.75±0.34	0.48±0.12	0.40±0.11	0.74±0.2	0.40±0.11	0.17±0.09	0.03±0.02	0.01±0.00
Kidneys	103±24	89.0±5.2	77.7±38.8	17.2±10.7	7.5±1. 8	170±40	147±14	111±61	19.1±11.7	7.5±1. 4
Stomach	2.01±0.41	2.55±0.69	2.87±0.55	2.24±1.08	1.91±0.95	0.74±0.16	0.60±0.15	0.46±0.23	0.26±0.38	0.17±0.21
Sm. Int.	3.14±0.66	2.29±0.69	1.32±0.68	0.42±0.12	0.31±0.07	1.45±0.32	1.46±0.54	1.03±0.56	0.16±0.09	0.09±0.04
Lg. Int.	0.86 ±0.66	1.86 ±0.25	3.34±0.66	1.18 ±0.52	0.55±0.19	0.36±0.06	0.74±0.14	2.35±0.28	1.35±0.65	0.73±0.39
Thyroid	0.79 ±0.17	0.77 ±0.25	0.75 ±0.17	0.74 ±0.27	0.88 ±0.13	0.34±0.13	0.22±0.05	0.20±0.10	0.20±0.11	0.19±0.06
Muscle	0.56±0.05	0.34±0.08	0.23±0.10	0.10±0.02	0.09±0.01	0.42±0.06	0.24±0.08	0.14±0.06	0.03±0.02	0.03±0.02
Blood	0.95±0.15	0.58±0.08	0.30±0.08	0.16±0.04	0.09±0.07	0.73±0.13	0.37±0.07	0.14±0.06	0.03±0.01	0.01±0.00
Bone	0.87±0.28	0.50±0.05	0.36±0.17	0.14±0.07	0.09±0.03	0.66±0.26	0.31±0.04	0.17±0.06	0.03±0.01	0.03±0.01
Brain	0.18±0.13	0.10±0.03	0.09±0.03	0.06±0.01	0.04±0.02	0.11±0.07	0.06±0.02	0.04±0.01	0.03±0.00	0.03±0.01
PC-3 PIP	16.5±4.8	17.2±4.3	18.3±4.3	15.8±2.4	13.6±3.3	24.3±7.5	25.6±6.6	19.6±11.5	22.9±3.4	19.7±4.9
PC-3 flu	1.09±0.21	0.80±0.11	0.57±0.21	0.28±0.10	0.20±0.08	0.73±0.18	0.48±0.10	0.25±0.10	0.05±0.01	0.06±0.03

[a]Mean ± SD (n = 5).

Table 4.

Paired label biodistribution of [^{211}At]GV-904 and [^{131}I]GV-904 in SCID mice bearing PC-3 PIP and PC-3 flu xenografts

Tissue	Percent injected dose per gram[a]					
	[^{211}At]GV-904			[^{131}I]GV-904		
	1 h	2 h	21 h	1 h	2 h	21 h
Liver	5.11 ± 4.13	3.80 ± 2.39	0.59 ± 0.21	5.16 ± 3.81	3.48 ± 2.35	0.24 ± 0.39
Spleen	9.51 ± 2.76	4.31 ± 1.96	2.07 ± 0.68	9.83 ± 3.28	3.41 ± 2.01	0.16 ± 0.07
Lungs	2.24 ± 0.51	1.96 ± 0.26	2.89 ± 0.93	1.39 ± 0.36	0.81 ± 0.37	0.03 ± 0.01
Heart	0.84 ± 0.27	0.76 ± 0.11	1.12 ± 0.27	0.46 ± 0.18	0.27 ± 0.14	0.02 ± 0.01
Kidneys	86.5 ± 15.5	87.7 ± 11.0	4.38 ± 3.46	121 ± 24	110 ± 37	3.03 ± 2.96
Stomach	1.64 ± 0.62	2.86 ± 0.67	9.36 ± 2.18	0.73 ± 0.26	1.03 ± 0.62	1.98 ± 3.10
Sm. Int.	33.9 ± 5.49	13.8 ± 10.9	1.51 ± 0.91	33.8 ± 6.4	14.2 ± 12.0	0.87 ± 0.92
Lg. Int.	0.75 ± 0.98	26.7 ± 15.3	8.55 ± 5.07	0.50 ± 0.65	21.3 ± 15.9	14.5 ± 8.1
Thyroid	0.51 ± 0.16	1.03 ± 0.26	3.74 ± 1.42	0.11 ± 0.13	0.31 ± 0.23	0.42 ± 0.35
Muscle	0.38 ± 0.16	0.21 ± 0.03	0.22 ± 0.06	0.31 ± 0.14	0.13 ± 0.03	0.03 ± 0.02
Blood	0.65 ± 0.33	0.35 ± 0.03	0.48 ± 0.13	0.46 ± 0.17	0.18 ± 0.07	0.02 ± 0.01
Bone	0.44 ± 0.10	0.40 ± 0.04	0.42 ± 0.16	0.33 ± 0.09	0.22 ± 0.07	0.02 ± 0.01
Brain	0.08 ± 0.02	0.08 ± 0.02	0.12 ± 0.03	0.05 ± 0.02	0.04 ± 0.02	0.01 ± 0.01
PC-3 PIP	22.7 ± 5.4	21.1 ± 6.16	12.1 ± 5.03	27.6 ± 7.6	24.7 ± 9.8	19.2 ± 7.3
PC-3 flu	0.80 ± 0.30	0.52 ± 0.05	0.84 ± 0.23	0.49 ± 0.23	0.22 ± 0.06	0.02 ± 0.01

[a]Mean ± SD (n = 5).